AD-A130 926 AFTERNOON EFFECT STUDIES PART 1(U) ROYAL AUSTRALIAN NAVY RESEARCH LAB EDGECLIFF J W HILL APR 83 RANRL-TN(EXT)-3/82-PT-1 1/1

UNCLASSIFIED F/G 20/1 NL

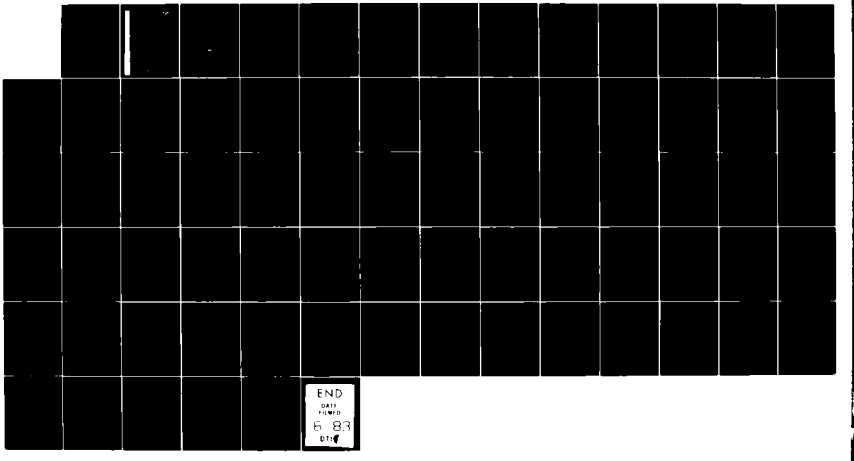

END
DATE FILMED
8 83
DTIC

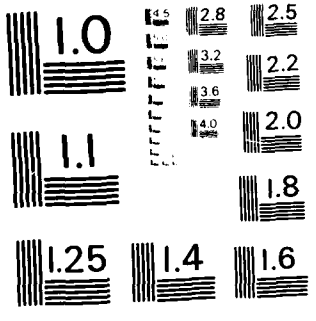

UNCLASSIFIED

RANRL T/N (EXT.) No. 3/82

AR Number: AR-002-699

DEPARTMENT OF DEFENCE SUPPORT
DEFENCE SCIENCE AND TECHNOLOGY ORGANISATION
R.A.N. RESEARCH LABORATORY
EDGECLIFF, N.S.W.

RANRL TECHNICAL NOTE (EXTERNAL) No. 3/82

"AFTERNOON EFFECT" STUDIES.

PART 1

BY

J. WARREN HILL

APPROVED FOR PUBLIC RELEASE

COPY No. 19

APRIL 1983

UNCLASSIFIED

DEPARTMENT OF DEFENCE

DEFENCE SCIENCE AND TECHNOLOGY ORGANISATION

R.A.N. RESEARCH LABORATORY

RANRL TECHNICAL NOTE (EXTERNAL) NO. 3/82

"AFTERNOON EFFECT" STUDIES, PART 1

J. WARREN HILL

ABSTRACT

"Afternoon effect" is a type of sonar performance loss encountered during the afternoons and evenings of calm sunny days. It is caused by a temperature rise near the top of the otherwise isothermal mixed layer, increasing the sound speed there and so refracting the sound rays downwards, away from the sonar target. The temperature rise profile is governed by wind speed, solar heating and other meteorological factors, so that afternoon effect prediction should become an extension of meteorological forecasting. However there is at present no established method for computing the temperature profile from the meteorological information.

A mixed-layer model is presented which appears to meet this need, subject to further testing. The influences of some key environmental factors are explored. An example of afternoon effect prediction is given, and the next steps towards a routine prediction facility are indicated.

POSTAL ADDRESS: The Director, RAN Research Laboratory,
P.O. Box 706, Darlinghurst, N.S.W. 2010

SUMMARY

"Afternoon effect" is a type of sonar performance loss encountered during the afternoons and early evenings of calm sunny days. It is caused by the development of a temperature rise near the top of the otherwise mixed layer, known as a "transient thermocline" or simply "transient". This increases the local sound speed, thus refracting sound waves downwards away from the target. In round terms the loss is or is not significant, depending on whether the sound speed at sonar projector depth does or does not exceed the speed at the bottom of the mixed layer. The mixed layer sound speed profile depends upon the temperature profile, which in turn is governed by wind speed, solar heating and other meteorological factors. Hence the prediction of afternoon effect should become an extension of conventional meteorological forecasting.

However there is as yet no established method for determining the diurnal temperature profiles from the meteorological data. A model is now presented which appears to meet this need subject to some further testing.

The model uses the standard one-dimensional eddy-diffusivity (K) equations for heat and horizontal momentum. These are closed by a third diffusivity-type equation in K itself, the generation term of which derives from the standard balance for turbulent kinetic energy. The last contains a prescription for turbulence dissipation, including a turbulence length scale, adapted from the literature. The three diffusion equations are solved by well-known numerical methods with computer assistance. The solutions are well-behaved and do not require smoothing.

The model is fitted to a data set acquired by the author, and then tested against established empirical rules for transient formation. K is found to decrease sharply with depth, through up to five decades, to a minimum at the transient bottom. The effect is to restrict sub-transient

diffusion of momentum and heat, totally at low wind speeds; the effect diminishes as the speed increases. This explains the "half-section of a wineglass" appearance characteristic of developed transients. The dissipation term in the turbulent energy balance is found to be comparatively minor, connoting severe stratification within the transient with gradient Richardson's number Ri exceeding one. This sets the model apart from others wherein Ri is limited to about 0.25.

The influences of a number of environmental factors are explored. Generally it is concluded that any factor which alters the balance between the effects of wind and solar radiation will have a major influence on transient formation.

An example of transient prediction is given, and the next steps towards a routine afternoon-effect prediction facility are indicated.

CONTENTS

FIGURES (in text)

FIGURES (in text)

TABLES (in text)

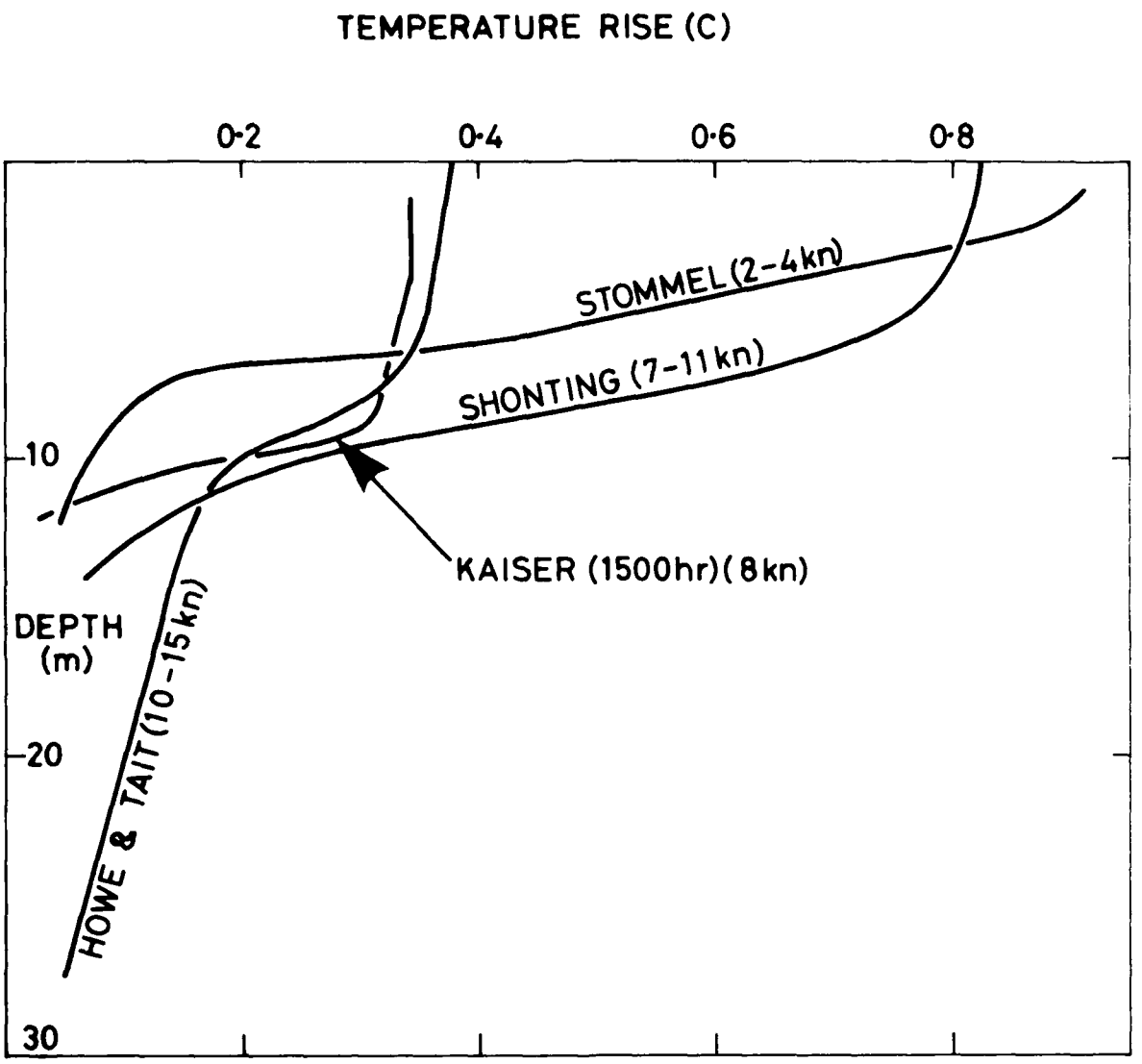

Fig. 1. Some observed temperature profiles in the nominally-mixed ocean layer, at 1600 local time except as indicated. Other bracketed figures are wind speed mean or range.

1. INTRODUCTION

1.1 Transient thermoclines

"Afternoon effect" is a loss of performance often suffered by surface-duct sonars under conditions of bright sunlight and low wind, so called because it usually peaks at that time of day. It is caused by the development of a temperature gradient close to the top of the mixed layer, representing the accumulation of solar heat in the absence of effective downward mixing by the wind. This temperature gradient produces a sound velocity gradient which refracts sound rays downward; in consequence the latter can escape from the surface duct altogether, causing the sonar performance loss already mentioned.

These near-surface temperature gradients are termed "transient thermoclines", often abbreviated simply to "transients", to distinguish them from the seasonal thermocline lying beneath the mixed layer. Transient observation is well-established in the literature. Sverdrup (1942, Table 32) gives diurnal surface temperature rises for tropical oceans, typically $1.6^{\circ}C$ for a nil to light breeze and $0.7^{\circ}C$ for a moderate to fresh breeze. These figures are for a clear sky; for an overcast sky they fall to $0.9^{\circ}C$ and $0.4^{\circ}C$ respectively. More recently, sets of temperature profiles taken during a single day have appeared in the literature, see for example Howe and Tait (1969), Kaiser (1978), Shonting (1964), and Stommel et al (1969). Fig. 1 shows a late-afternoon profile from each of these sources, marked with representative wind speed. A distinctive "half-section of a wineglass" appearance is seen to be common to all. To these may be added an isolated profile acquired by the author about 50 nm S.E. of Sydney, in April 1982 at 1300 local time. This is shown in Fig. 2; the distinctive wineglass shape had not developed by that time of day.

In most cases, however, the meteorological data is insufficiently

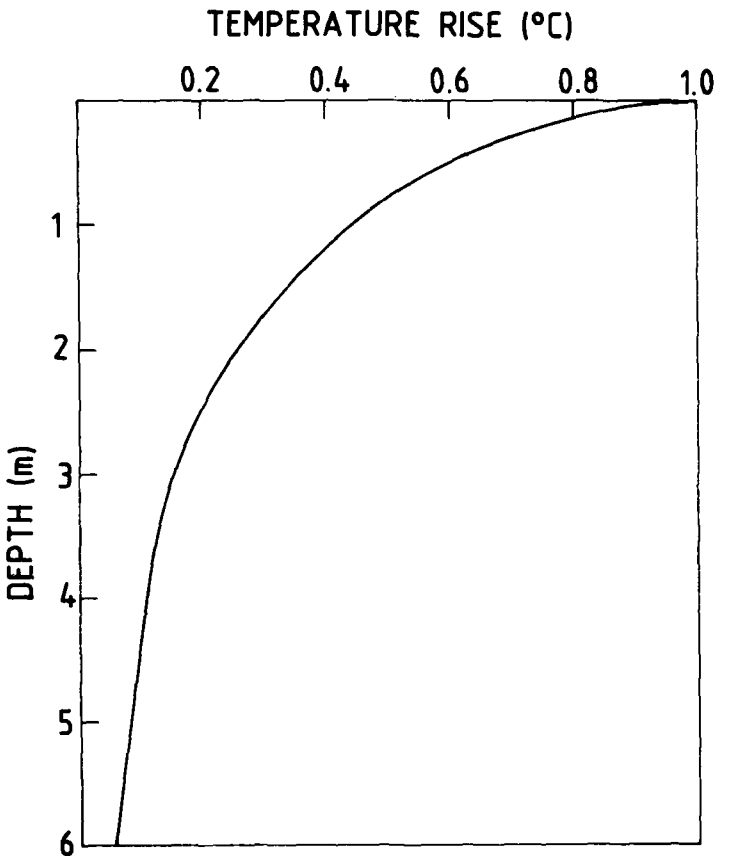

Fig. 2. Profile obtained by special slow-falling XBT from DTV SEAL on 6 Apr 1982 at 1300 local time, 50nm S.E. of Sydney. Wind speed 2-5 kn, cloud cover 1-2 eighths.

complete or precise to make any sort of theoretical check possible. Another difficulty often encounted is a major discrepancy between the water heat rise (profile area) and the cumulative entering heat inferred from the meteorological data; it is suspected that shallow temperature profiles taken close to the observing ship can be substantially distorted. Some high temperature rises under especially low wind conditions have been reported by Bruce and Firing (1974) (3.6°C) and by Romer (1969) (4.4°C). Although these data sets too are meteorologically lacking, it is noteworthy that with each the profiling equipment was deployed well away from the main experimental platform.

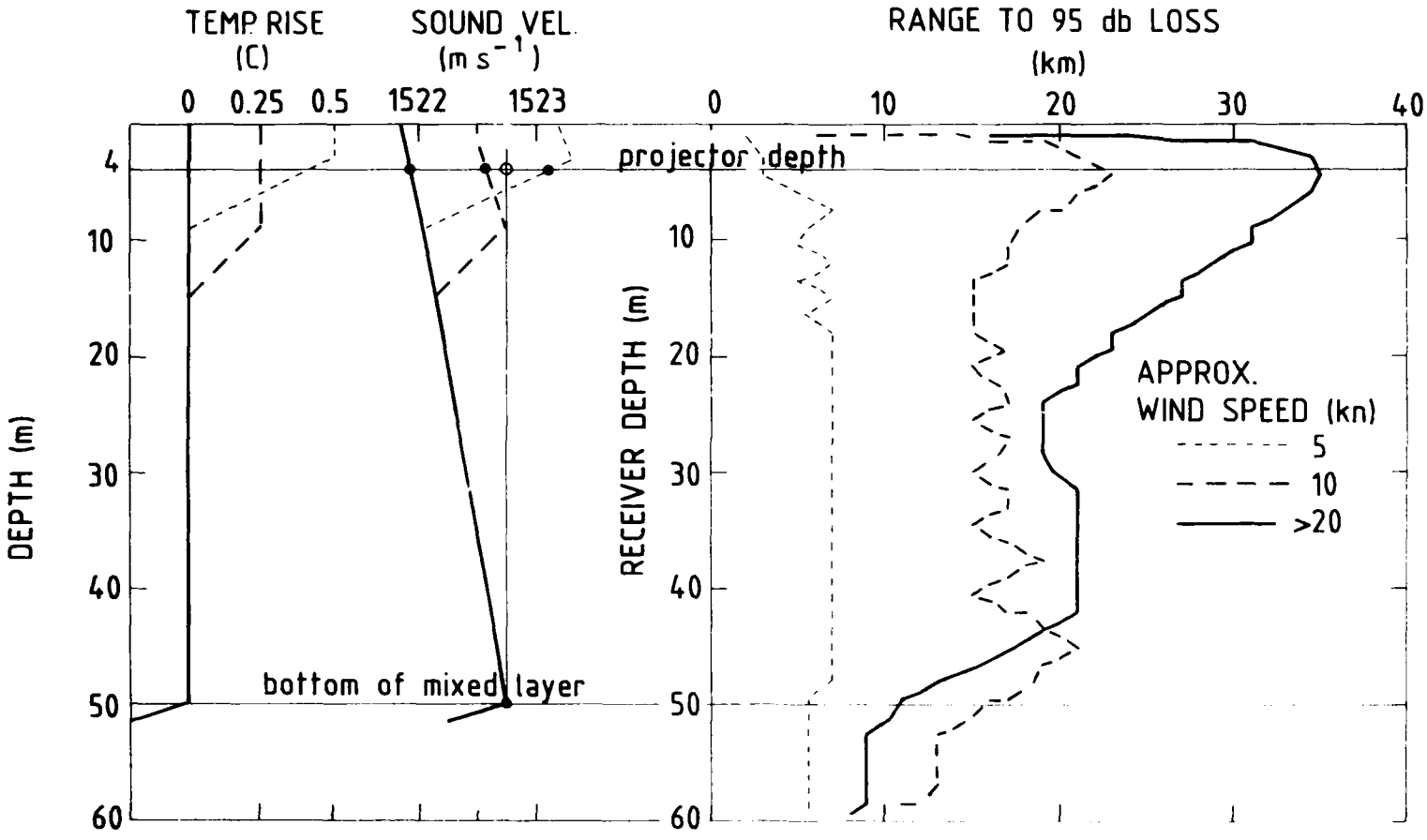

Fig. 3. Transients corresponding roughly to particular windspeeds, with corresponding sound velocity profiles, and hypothetical sonar ranges in terms of receiver depth.

1.2 Effect of transients on sonar performance

To study this, the first step is to convert the transient temperature profile over the full mixed-layer depth to a sound-velocity profile. Use is made of a sound-velocity equation such as that of Frye and Pugh (1971). From the resulting velocity profile may be calculated the transmission loss from source (sonar projector) to receiver (target). For active sonar the loss figure in dB is doubled because of the two-way transmission path. Service documents normally discuss the topic from the standpoint of ray theory. More precise results are obtained using mode theory, as explained typically by Pedersen and Gordon (1965). Mode theory takes account of the sound frequency used, and ascribes finite transmission losses to the "shadow zones" where according to ray theory sound does not penetrate at all. The benefit is obtained at the expense of extra computing complexity, however. It should also be pointed out that neither theory takes account of scatter at reflections from the surface due to roughness of the latter.

Fig. 3 shows two transients with corresponding sound velocity profiles. These profiles are idealized, but would correspond roughly to conditions of moderate solar heating and windspeeds of 5 and 10 knot. The undisturbed isothermal profile may be taken to represent a windspeed of over 20 knot. The sound velocities at the source depth are marked, and may be compared with that at the bottom of the mixed layer. Some hypothetical ranges corresponding to these profiles are shown in the figure, as a function of receiver depth. Here a 95dB loss from source to receiver is assumed, and mode theory is used. In the high-windspeed or isothermal layer case the sound velocity throughout the layer is less than the bottom value so that the duct operates to full advantage. Taking this as a basis

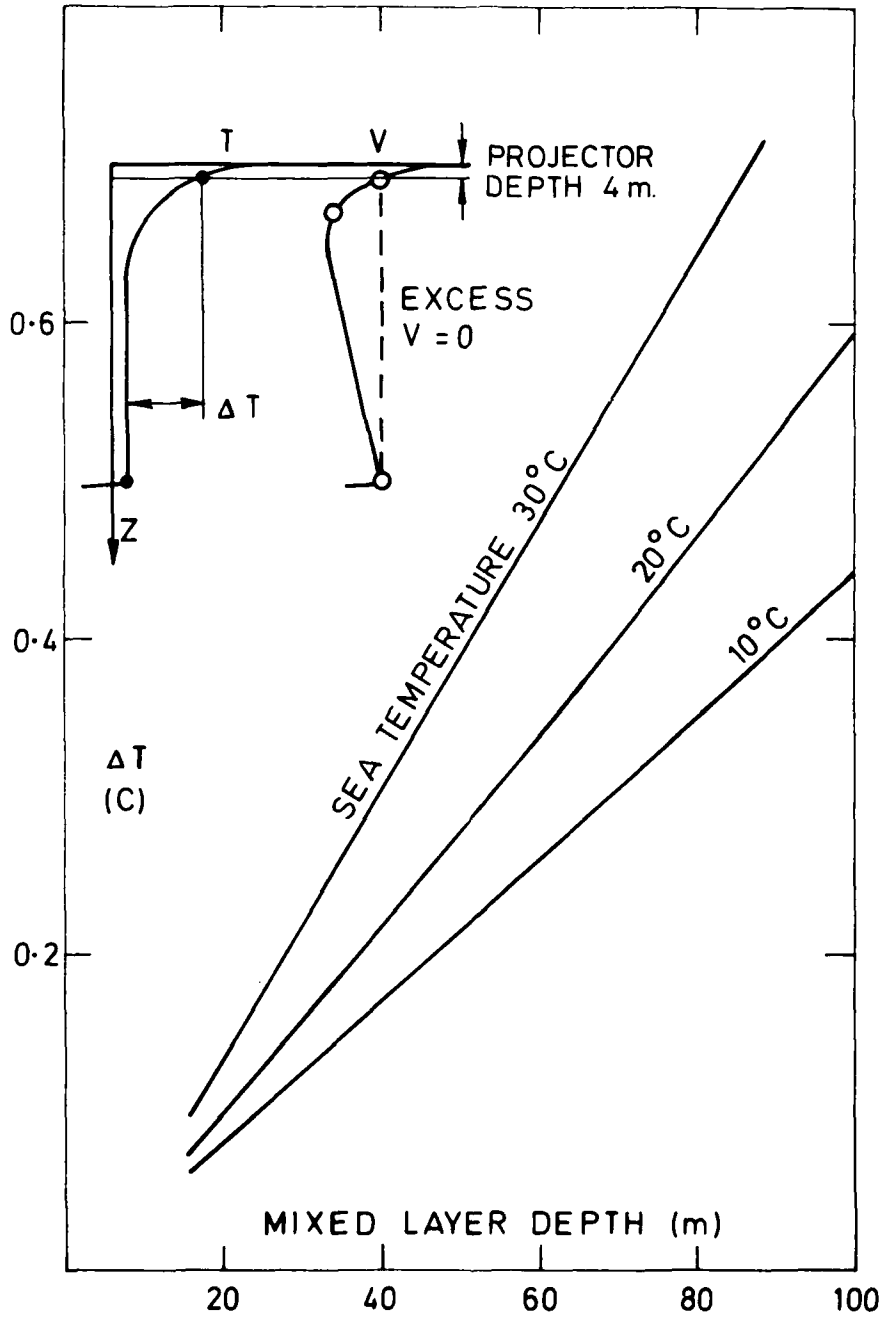

Fig. 4. Mixed-layer temperature differential for zero sound speed excess.

for comparison, at 10 knot windspeed the velocity at source and neighbouring levels is seen to be raised to the bottom value approximately. The range is found to be somewhat reduced, more particularly for the shallower receiver depths. At 5 knot windspeed the source velocity is seen to be well in excess of the bottom value; in this case the range is drastically reduced, from 20-30 km to about 7 km.

Clearly the influence of transients on acoustic transmission is complex. About the only simple generalization to emerge is that a "break point", beyond which sonar performance is seriously impaired, is reached when the sound velocity at the source depth becomes equal to that at the bottom of the mixed layer. Fig. 4 shows graphically the transient temperature rise at source depth 4m which produces this equality, in terms of the depth and the general temperature of the mixed layer; the curves are calculated using the sound velocity equation referred to earlier. Hence it is seen that the surface temperature rises cited from Sverdrup in Section 1.1, and the transients shown in Fig. 1, are all capable of disrupting sonar performance over a wide range of mixed-layer conditions.

The transient of Fig. 2, by contrast, is so shallow as to lie almost wholly above the source depth. Hence it should serve as an "overhead mirror", and if anything improve sonar performance by eliminating surface reflection with its attendant scatter.

1.3 The present studies

Although transient observations are well documented, very little on the theoretical side is to be found in the literature. Accordingly a new model has been devised to enable the progressive development of a transient during the day to be calculated from the forcing influences. The last being mainly meteorological, the prediction of sonar impairment by transient then becomes an extension of meteorological forecasting.

The model is successfully fitted to a limited set of profiling and meteorological data acquired by the author. It is then tested against two published sets of empirical rules for transient formation, each resting upon a large data base, and there is found to be broad agreement. The model indicates that the downward transmission of momentum and heat due to turbulent diffusion is shut off at the bottom of the transient, completely at low wind speed and progressively less as the speed increases. Hence the incoming solar heating is forced to accumulate above, producing the "half-section of a wineglass" appearance characteristic of well-developed transients. Other interesting aspects of transient formation are examined also.

The model is used to predict the effects of some important practical environmental changes on transient formation. The results of a typical afternoon effect prediction, made for a RAN exercise at the request of the Director of Oceanography and Meteorology, are given. It is planned that the new capability be added to the AUSRAPS sonar range prediction scheme operated by the RAN Meteorological Office at the Naval Air Station, Nowra NSW, under the authority of the Hydrographer RAN.

2. The model used

2.1 Diffusion equations for heat and momentum

These are based on the well-known empirical concepts of eddy diffusivity and eddy viscosity, symbol K, dimensions L^2T^{-1}; it has not so far been found necessary to distinguish between them. Salinity variation has not yet been considered, but could be through a further equation of the same type. The diffusion equations are frequently encountered in the literature, for example in the model of Mellor and Durbin (1975) with slightly different notation.

The heat diffusion equation is expressed in terms of temperature $T(t,z)$

$$\frac{\partial T}{\partial t} = \frac{\partial}{\partial z}\left(K \frac{\partial T}{\partial z}\right) + QR(t).\, RZ(z) \qquad (1)$$

where t is time, z is depth measured positively from the surface, and QR(t) is the penetrative heat flux (short-wave radiation) entering the surface. RZ(z) is the penetration/depth factor, or fraction of the entering radiant flux absorbed per metre at depth z; it is also the local temperature rise, in the absence of heat diffusion, due to unit cumulative flux.

The initial condition is a perfectly-mixed layer at sunrise, which provides a base level for temperature measurement: $T(0,z) = 0$ at all z. The boundary conditions for all t are: $z = 0$, $K_o \frac{\partial T}{\partial z} = QS(t)$; $z = z_m$, $\frac{\partial T}{\partial z} = 0$. Here QS(t) is the total non-penetrative heat flux from all sources entering the surface, K_o is the surface value of K, and z_m is the mixed-layer depth.

The momentum equation is analogously expressed in terms of the vector horizontal velocity $\underset{\sim}{W}(t,z)$. In standard complex algebra terms

$$\frac{\partial \underset{\sim}{W}}{\partial t} = \frac{\partial}{\partial z}\left(K \frac{\partial \underset{\sim}{W}}{\partial z}\right) - (i \times \underset{\sim}{W}) f \qquad (2)$$

The final term is the Coriolis force; $f = 2\Omega \sin\theta$, where Ω is the earth's angular velocity ($\frac{2\pi}{24}$ hr^{-1}) and θ is the latitude. The initial condition at all z is taken without loss of generality as $W(\cap,z) = 0$ *. The boundary conditions for all t are: $z = 0$, $K_o \frac{\partial \underset{\sim}{W}}{\partial z} = \underset{\sim}{\tau_o}(t)$; $z = z_m$, $\frac{\partial \underset{\sim}{W}}{\partial z} = 0$. The surface stress $\underset{\sim}{\tau_o}$ is expressed kinematically (dimension L^2T^{-2}) in terms of the wind speed U through the standard bulk formula

$$\left| \underset{\sim}{\tau_o} \right| = C_D \frac{\rho_{air}}{\rho_{water}} U^2$$

using any system of self-consistent units. The relative densities of air and sea-water are taken as .0012 and 1.02 respectively, and following Dillon and Powell (1979) the drag coefficient C_D is assumed to be .0013.

* for if at $t = 0$, $\underset{\sim}{W} = \underset{\sim}{W_o}$ at all z, all subsequent $\underset{\sim}{W}$ are simply increased by $\underset{\sim}{W_o} \exp(-i\underset{\sim}{f}t)$.

2.2 Diffusion equation for turbulence

The most widely accepted measure of turbulence is its kinetic energy E. Making the usual simplifications its local rate of generation in this one-dimensional model is, e.g. Mellor and Durbin (1975)

$$G_E = \underset{\sim}{\tau} \cdot \frac{\partial \underset{\sim}{W}}{\partial z} - g\beta Q - \epsilon \qquad (3)$$

where $\underset{\sim}{\tau}$ is the stress, g the acceleration due to gravity, β the volume coefficient of expansion, Q the heat flux diffused downwards, and ϵ the dissipation directly to heat. If turbulence storage and transport can be neglected then $G_E = 0$; this frequently-made assumption is considered later. However since the present situation involves substantial stratification and rapid change through the day, we wish to retain these features initially at least. One way is to set up a diffusion equation for turbulent energy, e.g. Kundu (1980, equ. 5)

$$\frac{\partial E}{\partial t} = \frac{\partial}{\partial z} \left(K \frac{\partial E}{\partial z} \right) + G_E \qquad (4)$$

The disadvantage here is that the additional variable E is introduced, so that a final closing equation is still required. Some modellers, e.g. Kundu (1980) and Marchuk et al (1977) add yet another diffusion equation, in ϵ, making a further closing equation necessary still.

The author instead proposes one single equation for closing (1) and (2), based entirely upon the turbulent diffusivity K (t,z). By analogy with (4) this should be a diffusion equation of the form

$$\frac{\partial K}{\partial t} = \frac{\partial}{\partial z} \left(K \frac{\partial K}{\partial z} \right) + G_K \qquad (5)$$

treating K as a scalar property which can be stored, diffused and generated - in fact as an alternative measure of turbulence to E.

This approach needs a suitable parameterization of G_K . Accordingly we postulate a one-to-one correspondence between G_K and G_E which could, of course, involve some function of K rather than K itself. Given this flexibility, dimensional analysis leads directly to the relationship

$$G_K = AK^{\frac{1}{2}} (\text{sign}) \mid G_E \mid^{\frac{1}{2}} \tag{6}$$

Here A should be a universal constant since nil fresh dependence on bulk parameters (e.g. Richardson's number) is postulated. Both positive and negative values of G_E are to be catered for, hence the device of taking the square root of the magnitude of G_E and then reinstating the original sign.

Henceforth it is convenient to re-express (3) as

$$G_E = K(VG^2 - BG - DIS) \tag{7}$$

with the velocity gradient $\left|\frac{\partial W}{\partial z}\right|$ written as VG, the buoyancy gradient $g\frac{\partial T}{\partial z}$ as BG, and a modified form of the dissipation, ε/K, as DIS. We note that Richardson's number (Ri) is BG/VG^2 . Combining (6) and (7) gives

$$G_K = AK\ (\text{sign}) \mid VG^2 - BG - DIS \mid^{\frac{1}{2}} \tag{8}$$

When (8) is inserted in (5) the complete diffusion equation for diffusivity becomes

$$\frac{\partial K}{\partial t} = \frac{\partial}{\partial z} \left(K \frac{\partial K}{\partial z}\right) + AK\ (\text{sign}) \left| VG^2 - BG - DIS \right|^{\frac{1}{2}} \tag{9}$$

with K not permitted to fall beneath the molecular level.

Under neutrally buoyant conditions ($\beta = 0$) and with DIS ignored, (9) reduces to

$$\frac{\partial K}{\partial t} = \frac{\partial}{\partial z} \left(K \frac{\partial K}{\partial z}\right) + AK.VG$$

These are the principal terms in a model developed by Nee and Kovasznay (1969) for such conditions. From experimental results they assign the value 0.133 to A. This value turns out to be suitable for the present work and is adopted henceforth.

Initial and boundary conditions are required for (9). The former, at sunrise, follow an overnight period of surface cooling and consequent overturning which is usually sufficient to mix the upper layer completely. In these circumstances K is assumed to commence at some value K_i, uniform throughout the mixed layer on account of the overturning, and well above molecular level on account of the energy derived from both the overturning and the overnight wind stirring. The present model is not yet sufficiently advanced to determine K_i from overnight conditions. Instead a traditional formula is adapted from Sverdrup (1942, p. 494)

$$K_w \ (m^2 hr^{-1}) = \left.\begin{matrix} 0.41\ W^2 \\ 0.05\ W^3 \end{matrix}\right\} \text{ whichever is less} \qquad (10)$$

where W (knot) is the sunrise wind speed. K_i is generally made equal to K_w; departure from this is explored in Section 4.

The boundary conditions adopted for (9) at the surface and at the bottom of the mixed layer are both $\frac{\partial K}{\partial z} = 0$, implying zero vertical flux of K at these levels. Here the equation is applied by expressing VG and BG as the known fluxes of momentum and heat respectively, divided by K. In this way K is found right up to the boundaries, improving the precision of heat and momentum flux calculations made nearby.

This modelling approach is less radical than it might at first seem. If turbulence storage and transport effects were small enough to

neglect, then (5) would reduce to $G_K = 0$ just as (4) would to $G_E = 0$; (6) indicates these conditions to correspond. We are in effect starting from the original approximation $G_E = 0$ and adding empirical terms representing turbulence storage and transport; the unconventionality lies in basing these additions upon K rather than E, or for that matter upon ε. As terms in a diffusion equation, $\frac{\partial K}{\partial t}$ and $\frac{\partial}{\partial z}(K\frac{\partial K}{\partial z})$ may not have the physical standing of $\frac{\partial E}{\partial t}$, but they do not seem to be any less plausible than $\frac{\partial}{\partial z}(K\frac{\partial E}{\partial z})$, $\frac{\partial \varepsilon}{\partial t}$ or $\frac{\partial}{\partial z}(K\frac{\partial \varepsilon}{\partial z})$. However doubtful the new additions may be, it is surely better to take some account of turbulence storage and transport rather than none at all.

2.3 Prescription for dissipation

This is the only means provided for fitting the model to observed data, see again (9).

Dissipation thinking for the present model was influenced by early experience (Hill, 1980) when dissipation was omitted altogether. A reasonable modelling fit was obtained at low wind speed, deteriorating at higher speeds but not disastrously. As a result, present practice is to make the dissipation adjustable from zero upwards. Three different prescriptions are examined, each with its multiplying factor of adjustment. We select among these and adjust to give best fit of the model to observational data.

Dissipation is commonly considered to be linked to turbulent kinetic energy through the formula

$$\varepsilon \propto E^{3/2}/L \tag{11}$$

where L is a length scale provided by the environment. E in turn is often linked to K through another formula

$$K \propto E^{\frac{1}{2}}L \tag{12}$$

Elimination of E leads to

$$DIS \equiv \varepsilon/K = (K/L^2)^2 \cdot F \tag{13}$$

where we introduce a numerical "dissipation factor" F to be adjusted later.

As an alternative to (12), Bradshaw et al (1967) replace E in (11) by the stress magnitude $|\tau|$. This leads to

$$DIS \propto |\tau|^{3/2}/KL = (K/L^2)^{\frac{1}{2}} \cdot VG^{3/2} \cdot F \tag{14}$$

A third possibility is simply to declare the turbulent energy dissipation rate to be a fixed proportion of the generation rate.

Denoting the fixed proportion by F

$$DIS = (K.VG^2.F)/K = VG^2.F \qquad (15)$$

However if turbulence storage and diffusion were negligible this would be equivalent to fixing Ri, which is theoretically unrealistic. Evidently these three prescriptions for DIS are members of the one family

$$DIS = (K/L^2)^P \cdot VG^{2-P} \cdot F \qquad (16)$$

with the "dissipation index" P taking values 2, ½ and 0 respectively; this is the widest range possible without incurring negative indices.

To obtain a length-scale L we follow Mellor and Durbin (1975), who propose the ratio of the first- to zeroth-order moments of the $E^{\frac{1}{2}}$ - z field. Substituting $|\tau|$ for E as above gives

$$L = \int_0^{z_m} |\underset{\sim}{\tau}|^{\frac{1}{2}} . \, zdz \Big/ \int_0^{z_m} |\underset{\sim}{\tau}|^{\frac{1}{2}} . \, dz \qquad (17)$$

2.4 Method of solution

Equations (1), (2), and (9) are solved numerically with both time and depth divided into discrete intervals. The semi-implicit (Crank - Nicolson) form of the finite-difference method is used, as explained typically by Razelos (1973, Section 4). Each of (1), (2) and (9) becomes a set of simultaneous equations, with each member of the set representing the interaction of three adjacent depth elements over a single time interval. The set is solved by tridiagonal Gaussian elimination. This procedure is straightforward for the linear equations (1) and (2), even though the latter involves complex algebra, but a difficulty arises with (9) on account of its non-linearity in K. The last is overcome by expressing each K (t,z) as the sum of an already-obtained approximate solution and an unknown, supposedly small, correction; the equations are reformulated in terms of the latter and are thereby linearized. The resulting corrections are applied to the approximate solutions, and the process is iterated until all corrections become acceptably small. Some 20 iterations are usually found necessary. The dissipation scale L is calculated in the same iterative loop.

Immediately following the solution of (1) any positive temperature gradient is removed by "pooling" the least possible number of nearby elements. This is to simulate the natural overturning which occurs early and late in the day when surface cooling predominates. Velocity and diffusivity are pooled also. The latter is increased to reflect the turbulent energy gained from overturning, using an adaptation of (6).

At present the standard computing timestep is 5 min. For practical temperature prediction work the depth elements are made 1 m thick to 20 m, thence 2 m to 30 m, 5 m to 50 m, and 10 m to the bottom of the mixed layer if this has not already been encountered. However for systematic studies the upper element thicknesses are adapted to the wind speed. At the

lowest speed considered here, 5 knot, the near-surface detail is found to require ½ m elements as far as 15 m. At the highest, 15 knot, little happens close to the surface but a computational instability often encountered in this type of numerical analysis is found to enter; this difficulty is avoided by amalgamating all of the 1 m elements to 2 m.

"Spot" or instantanous data values are entered, usually on an hourly basis. The program interpolates between successive values to suit each intermediate computing timestep. Two-hourly outputs are usually sufficient. The solutions are found to be well-behaved and not to require smoothing.

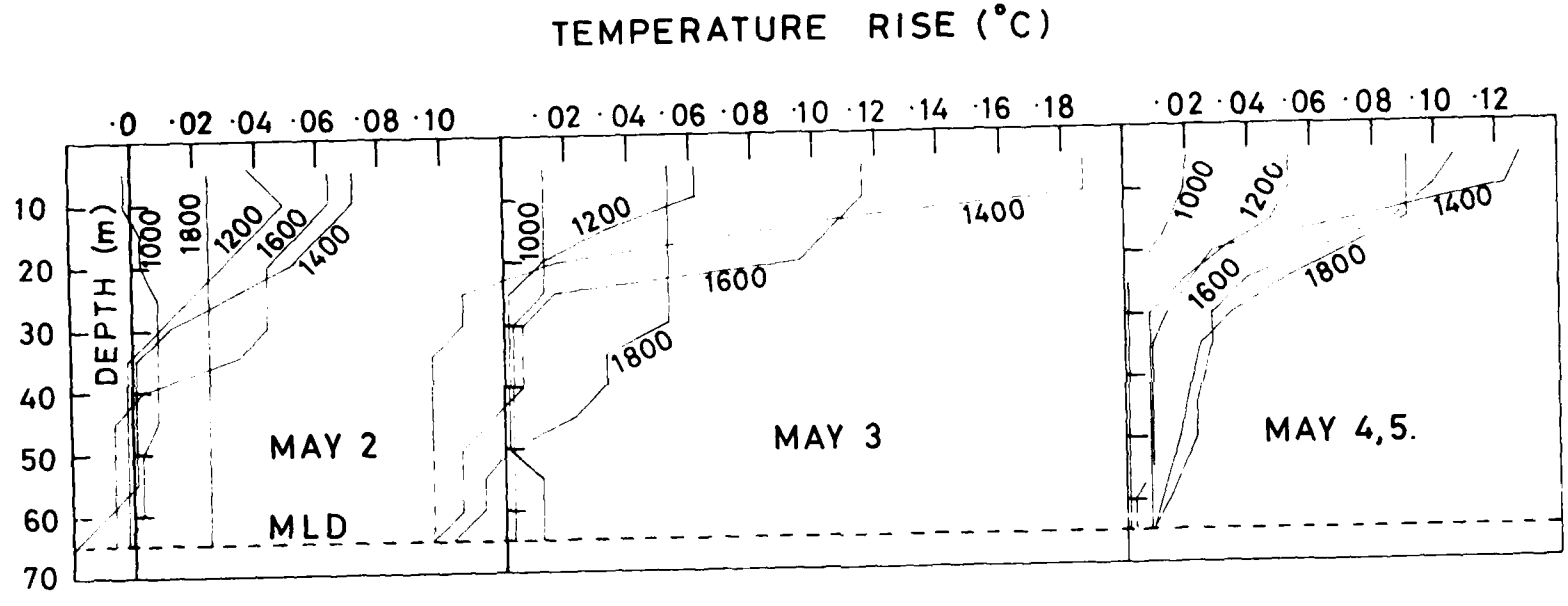

Fig. 5. HMAS DIAMANTINA cruise May 1976, temperature profiles obtained by XBT. Base temperatures have been adjusted to give overall heat balance.

3. Modelling an observed transient

3.1 Observational data

In May 1976 the research ship HMAS DIAMANTINA, since decommissioned, occupied three stations in the Indian Ocean successively for five days each. Mixed-layer temperature profiles were taken at two-hourly intervals, continuously over the time on station, using standard Sippican expendable bathythermographs (XBT s). All necessary meteorological observations were made at the same times.

These XBT traces suffer from a slow recorder start, causing the top 5 m of the profile to be lost. Moreover the warranted absolute accuracy is $0.2^{\circ}C$, far outside that needed for the present studies. However within any one record the level of coherence is considerably better, and traces may be digitized to $0.01^{\circ}C$ using simple magnifying techniques only. To overcome the lack of an absolute temperature baseline, one is inferred for each profile to make the water heating (profile area) equal to the net input heating from all causes, cumulatively from sunrise to the hour of the profile.

Table 1 shows the general conditions obtaining at one of the stations, at location $12\text{-}13^{\circ}S$, $105\text{-}106^{\circ}E$. Heating was only moderate on account of the winter season, and cooling high on account of the brisk unceasing winds. The corresponding temperature profiles are shown in Fig. 5. Those for May 1 are virtually isothermal, not surprisingly in view of the high winds, and are accordingly omitted. On May 2 there was heavy overcast, producing temperature rises unsuitably small for analysis. The May 3 profiles are found to be anomalous, giving peak water heats much higher than can be reconciled with the apparent input heating; when a profile is moved horizontally to give the correct included area, its lowest temperatures are seen to go substantially negative. This unrealistic behaviour is not at present

TABLE 1

HMAS DIAMANTINA CRUISE 1-5 MAY, 1976

PRINCIPAL DAYTIME FEATURES

DATE MAY	MIXED LAYER DEPTH (m)	TRUE WIND SPEED (knot)	TRUE WIND DIRECTION* (deg)	SHIP OVER GROUND SPEED (knot)	SHIP OVER GROUND DIRECTION* (deg)	CLOUD COVER (eighths)	HEAT BALANCE QUALITY	REMARKS
1	62-70	15-33	290					all XBT s isothermal in mixed layer
2	65-70	10-16	270-280	1.2-1.6	250-270	4-6	good	ship drifting freely
3	60-74	16-18	255-300	1.3-1.6	120	2-4	poor	
4	67-75	9-19	240-270	1.0-1.4	Various	~2	good	data for the two days composited
5	60-70	10-16	280-300	1.3-3.0	Various	~2	good	data for the two days composited

* all directions are that of the velocity vector concerned, i.e. along the motion.

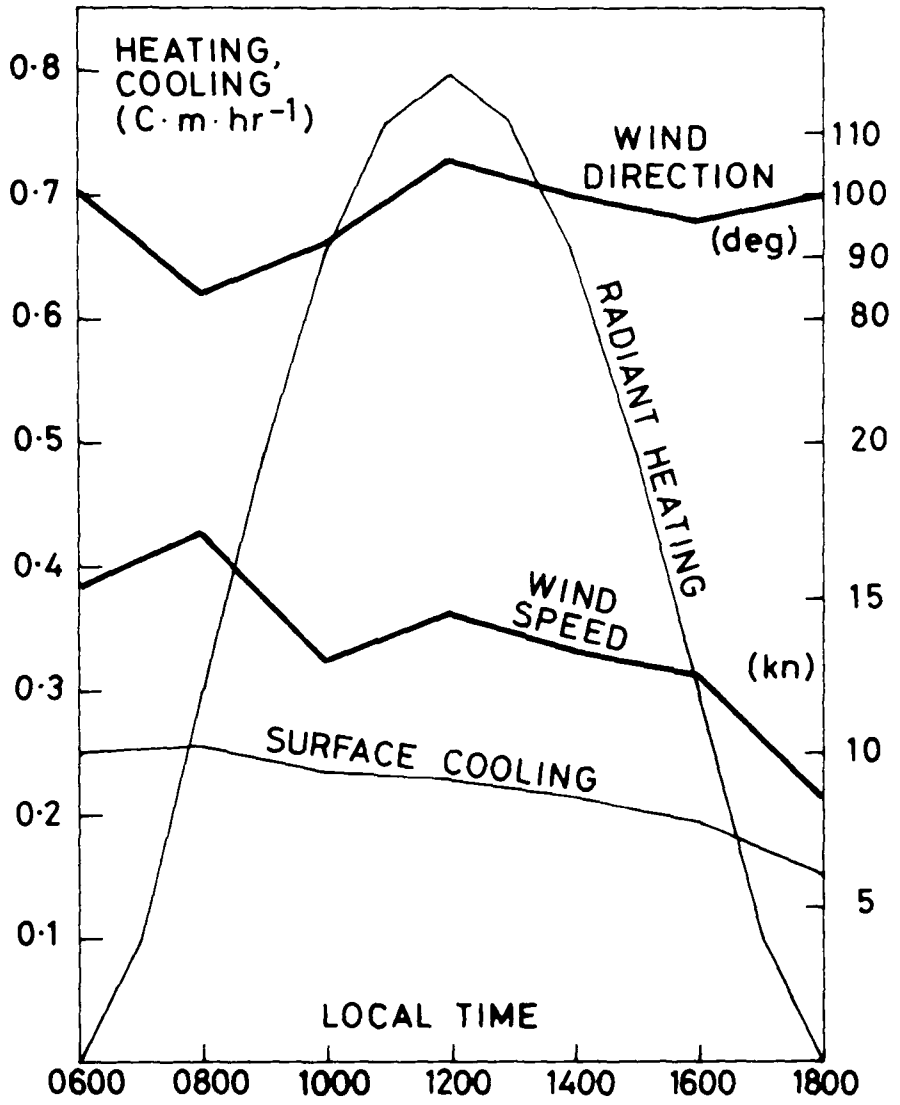

Fig. 6. HMAS DIAMANTINA cruise May 4/5 1976, composited meteorological data : wind speed and direction, and inferred rates of radiant heating and surface cooling.

understood. However on May 4 and 5 conditions were more favourable, with strong heating; these profiles tend to coincide fairly well at depth. Since the results for the two days are similar, they are composited in order to improve accuracy. This data set is now selected for model fitting.

The meteorological observations were made by trained naval personnel, and comprised: apparent wind speed by hand-held anemometer, later corrected to true speed from SATNAV fixes of ship's position; true wind direction inferred from wave front orientation; dry- and wet-bulb air temperatures; sea temperature by bucket; and weather state generally, including cloud cover. From these are calculated the entering radiant heat and the net long-wave radiant surface cooling using charts prepared by James (1966, Figs. 23 and 26), also the net air-sea heat exchange according to the parameterisations of Friehe and Schmitt (1976). Fig. 6 shows the penetrative radiant heating and the overall surface-cooling rates, also the wind speeds and directions, all composited for May 4 and 5. The derived heat unit used, C.m, enters naturally when estimating water heat as the area under a temperature profile scaled in ^{o}C and m: 1 C.m = 4.0 MJ m^{-2}.

Data is also required on water clarity for calculating the depth distribution of heat delivered by short-wave radiation, the RZ term in (1). Since no measurements were made from HMAS DIAMANTINA, the optical classification Oceanic Ib is estimated from a regional map provided by Jerlov (1968, Fig. 50). For each classification Jerlov tabulates the fraction of entering radiant flux which remain unabsorbed at particular depths (Table XXI). This data for classification Oceanic Ib is shown in Table 2, and that for the middle-range coastal classification Coastal 5 is added for comparison. For the present purpose it is necessary to draw a smooth curve through the tabled data points; the RZ function is then obtained by differentiating with respect to depth. Difficulty was experienced at first with manual curve drawing

TABLE 2

UNABSORBED PERCENTAGE OF RADIANT FLUX AT PARTICULAR DEPTHS, FOR REPRESENTATIVE OCEANIC AND COASTAL TYPE WATERS

(AFTER JERLOV (1968) TABLE XXI)

DEPTH (m)	UNABSORBED PERCENTAGE OF RADIANT FLUX	
	Oceanic Ib	Coastal 5
0	100	100
1	42.9	27.8
2	36.0	16.4
5	25.8	4.6
10	16.9	0.69
20		0.02
25	7.7	
50	1.8	
75	0.42	
100	0.10	

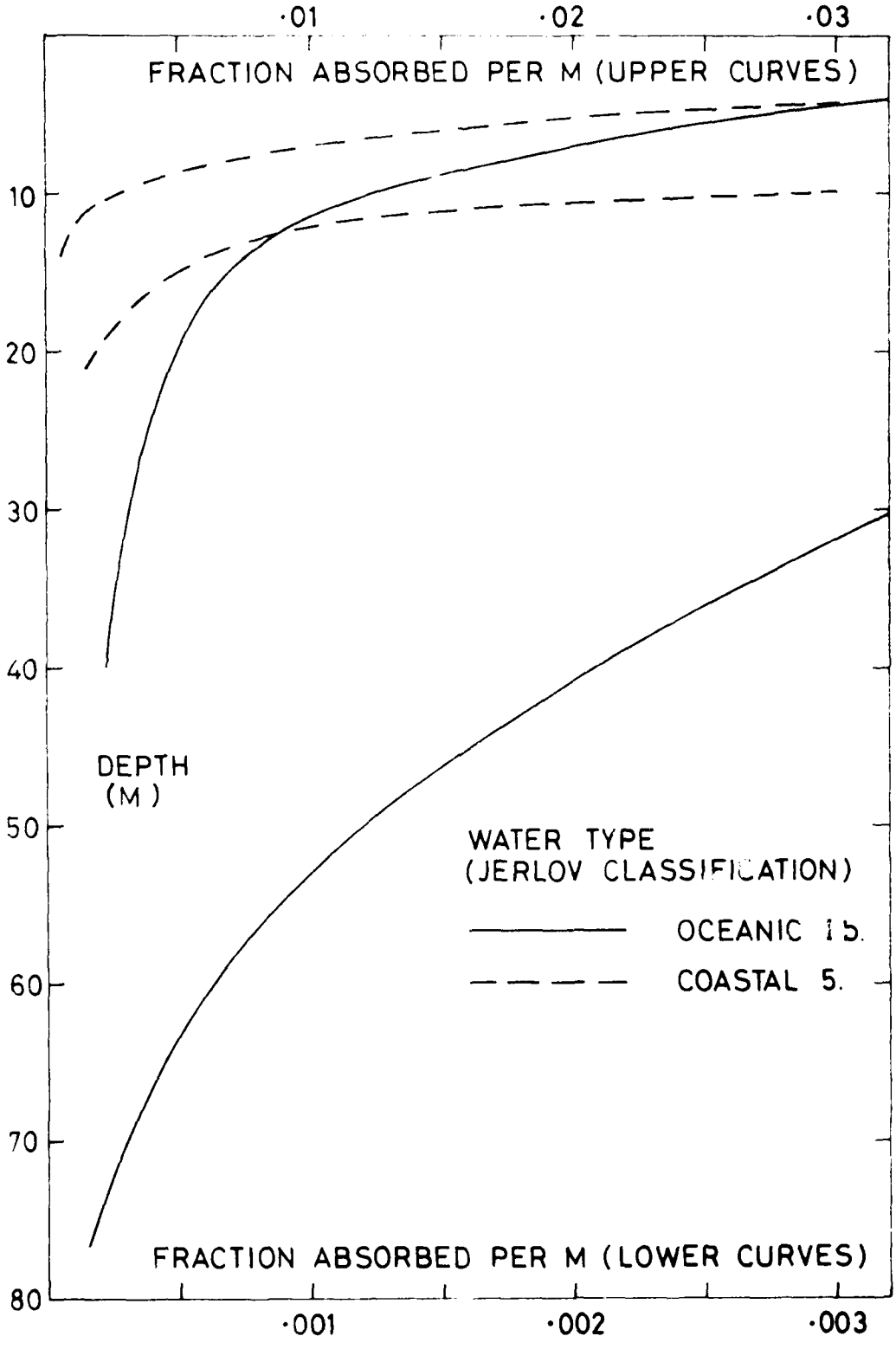

Fig. 7. Radiant penetration - depth factors (RZ) for representative oceanic and coastal type waters.

leading to roughnesses in the RZ curves, leading in turn to anomalies in the graphed model results. Hence a computerised method of interpolation was sought instead. The standard polynominal and cubic spline methods can produce unrealistic ("wiggly") curves when the datum points are sparse as in this case. Accordingly a new method has been developed, giving a curve more acceptable to the trained eye, still with continuity of first and second derivatives throughout. The smooth RZ curves then obtained are shown in Fig. 7. This development is of some general interest and is proposed for external publication (Hill, 1983).

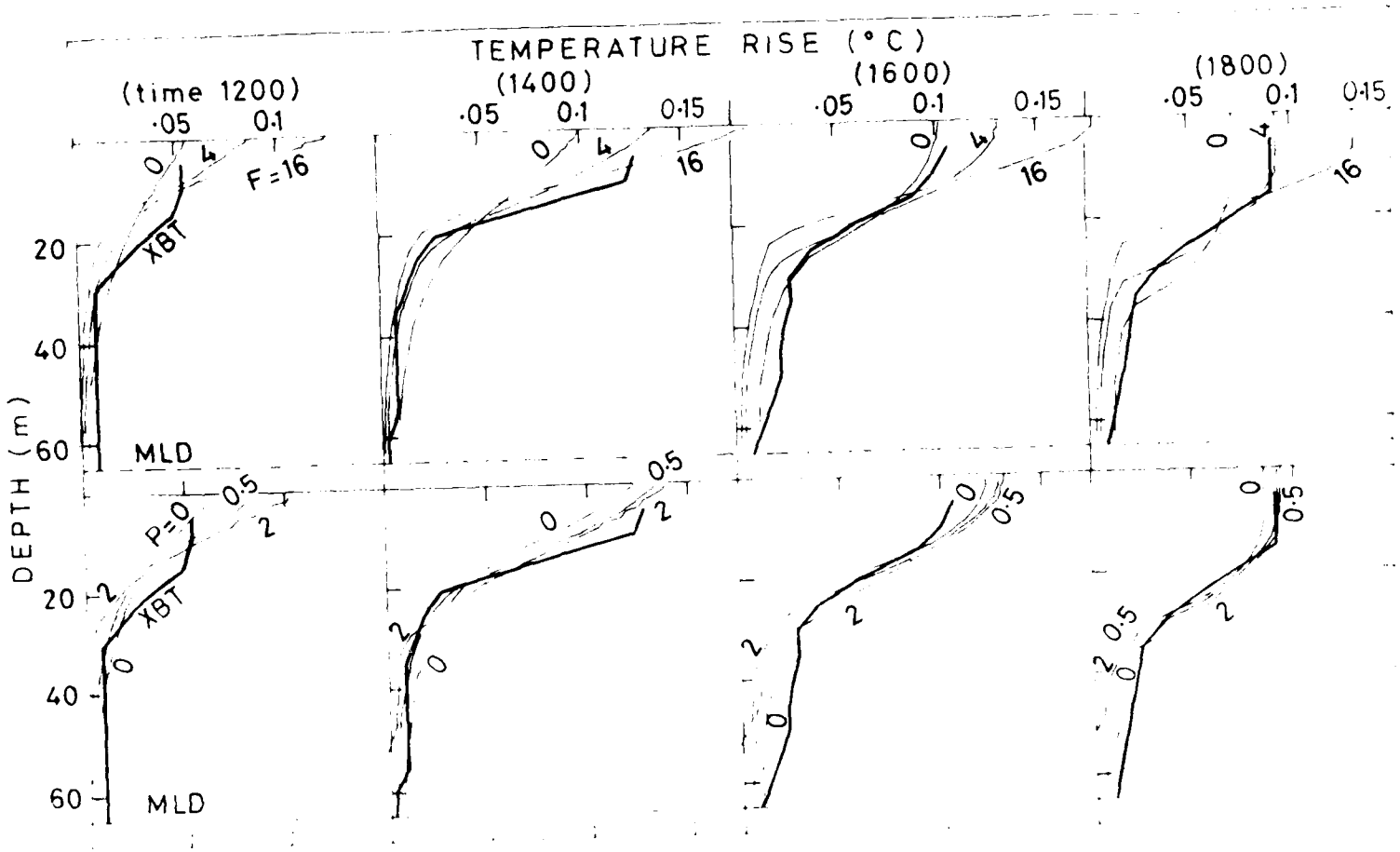

Fig. 8. RRS DISCOVERY cruise 56, 1974. Upper panel: composites XBT temperature profiles (to 60 m) at 1200, 1400, 1600 and 1800 local times, from Fig. 3; also corresponding modelled profiles (light line) with dissipation index F = 0, 4 and 16 values as marked, using meteorological data of Fig. 6. Water assumed to be of oceanic Ib model type. Lower panel: the same except that the model profiles are for P = 0, 0·5 and 2 and 0, which applied at [illegible] respectively.

3.2 Fitting the model to the data

The foregoing meteorological data are now entered in the model. For a first trial the dissipation index P is set at 0.5 and F_0 at 0 (no dissipation), 4 and 16 successively. The upper panel of Fig. 8 shows the resulting temperature profiles at times 1200, 1400, 1600 and 1800. These profiles are formed by connecting the computed points with straight lines without any smoothing, or omission of points. The processed XBT profiles from Fig. 5 are added for comparison.

There is seen to be broad general agreement between observation and model, improving as the day proceeds. The progressive deepening of the transient and the late-afternoon overturning near the surface are modelled realistically. While the modelled profiles do not fit well enough to fix F_0 precisely, inspection of their upper regions enables F_0 to be bounded; clearly zero represents too little dissipation and 16 too much. We provisionally set F_0 at the intermediate level 4.

The other two dissipation indices give broadly similar results when F_0 is varied through an appropriate range. The lower panel of the figure shows the results for all three indices, each with F_0 optimised in the foregoing manner. Naturally the upper parts of these curves differ only slightly. Beneath the transient however, in what we may regard as the "stem" of our wineglass, there are significant differences, P = 0 giving the most heat penetration and P = 2 the least. Indeed with the latter some deep negative temperatures built up in the early morning, before the radiant heating becomes significant, remain undisturbed all day. However with all three values of P these temperature rises are small. Their differences with the "observed" values should not be taken too seriously because of possible errors in the latter, arising from the method of temperature base adjustment.

The extreme P-values 2 and 0 can be criticised on other grounds. The former gives noisy results near the surface and introduces a strong dependence upon the doubtful length scale L. The latter gives indifferent near-surface performance in the early afternoon, and in Section 4 is found to lead to computing difficulties. On balance, P = 0.5 with F 4 seems to be the best present choice among the three.

Summarising, we have a range of models to choose from, all broadly successful, differing only in the prescription adopted for turbulence dissipation. The implication is that dissipation plays only a minor part in the whole process of transient development. We shall see more direct evidence of this later, and meanwhile pass to the consideration of further input data.

4. Testing against empirical rules for transient formation

The R.N. Director of Naval Oceanography and Meteorology (DNOM, 1968) has assembled a data set comprising some 25000 bathythermograph (BT) soundings, mostly accompained by the relevant meteorological observations. The BT swere taken during 1964-1967 from R.N. weather ships on Ocean Weather Stations INDIA and JULIET, located in the North-East Atlantic Ocean at latitudes 59°N and 52½°N respectively. The data was analysed by DNOM and the following empirical rules for transient behaviour were laid down

(1) The depth of formation, to the top of the transient, is 3, 6 or 9 m for a mean wind speed of 5, 10 or 15 knot respectively, over the three hours prior to formation.

(2) Significant transients, i.e. those clearly visible on BT traces, are commonly about 6 m thick, rarely less than 3 m and not often more than 9 m.

(3) For wind speeds over 15 knot transient formation is unusual.

Another data set has been assembled by Tabata, Boston and Boyce (1965) from the records of Ocean Weather Station PAPA located in the North Pacific Ocean at latitude 50°N. This is for the period 1956-1959 inclusive, and for the summer months only (April through August) when most transients form. The cited data comprises

(i) the depth to the top of the shallowest thermocline (i.e. transient) of a BT always taken at 1620 local apparent time, and

(ii) the average of 5 wind speeds measured over the preceding 12 hours.

TABLE 3

TRANSIENT-DEPTH/WIND-SPEED RELATIONSHIP AFTER

TABATA ET AL (1965, FIG 3)

WIND SPEED RANGE knot	NO. OF PLOT POINTS	DEPTH TO TOP OF SHALLOWEST THERMOCLINE AT 1620 LOCAL APPARENT TIME (m)		
		Range	Mean	Std. deviation
4-6	27	0-10 (excl. 2 points)	3	2
9-11	53	0-17	6	2
14-16	38	5-20 (excl. 1 point)	12	2

Any depths not clearly attributable to the day's wind speeds are rejected. The results are reported as points on a depth/wind-speed linear plot (Tabata, Fig. 3) extending to about 40 m and 30 knot, with the straight line of best fit superimposed. The last is not used here because the range of wind speed covered is wider than that of present interest; instead three groups of plot points are selected in the vicinity of the key DNOM wind speeds, viz. 5, 10 and 15 knot. The average depths for the three groups are set out in Table 3, each with standard deviation. They are seen to be the same as those found by DNOM, except that at 15 knot wind speed the depth is 12 m instead of 9 m.

Thus there is prospect for testing the model, already adjusted to fit data for a narrow wind speed range, over a much wider range even if the test is only a "broad-brush" one. To this end a sample ocean location is taken at latitude 53°N representing all the OWS s cited. A fine midsummer day with cloud cover not exceeding two-eighths is assumed, and the remaining model inputs are based on climatological data for the North-East Atlantic Ocean region. The total radiant heating for the day is estimated at 7.1 C.m*, with noon peak 0.77 $C.m.hr^{-1}$, and the total surface cooling rate at $(0.06 + 0.005\ W)$ $C.m.hr^{-1}$ where W is the wind speed in knots. The general mixed-layer temperature is taken as $15^{\circ}C$, corresponding to a volume coefficient of expansion 0.0002 C^{-1}. As before the water optical classification is taken to be Oceanic Ib. Wind speeds of 5, 10 and 15 knot are examined.

This package of idealised meteorological conditions is modelled as before with P = 0.5. The results are shown in Fig. 9, in a separate row for each wind speed; the major influence of the last upon temperature rise and transient depth is immediately apparent. Two-hourly temperature profiles with F = 4 are plotted at the left-hand side of each row, with temperature

---

* See again Section 3.1

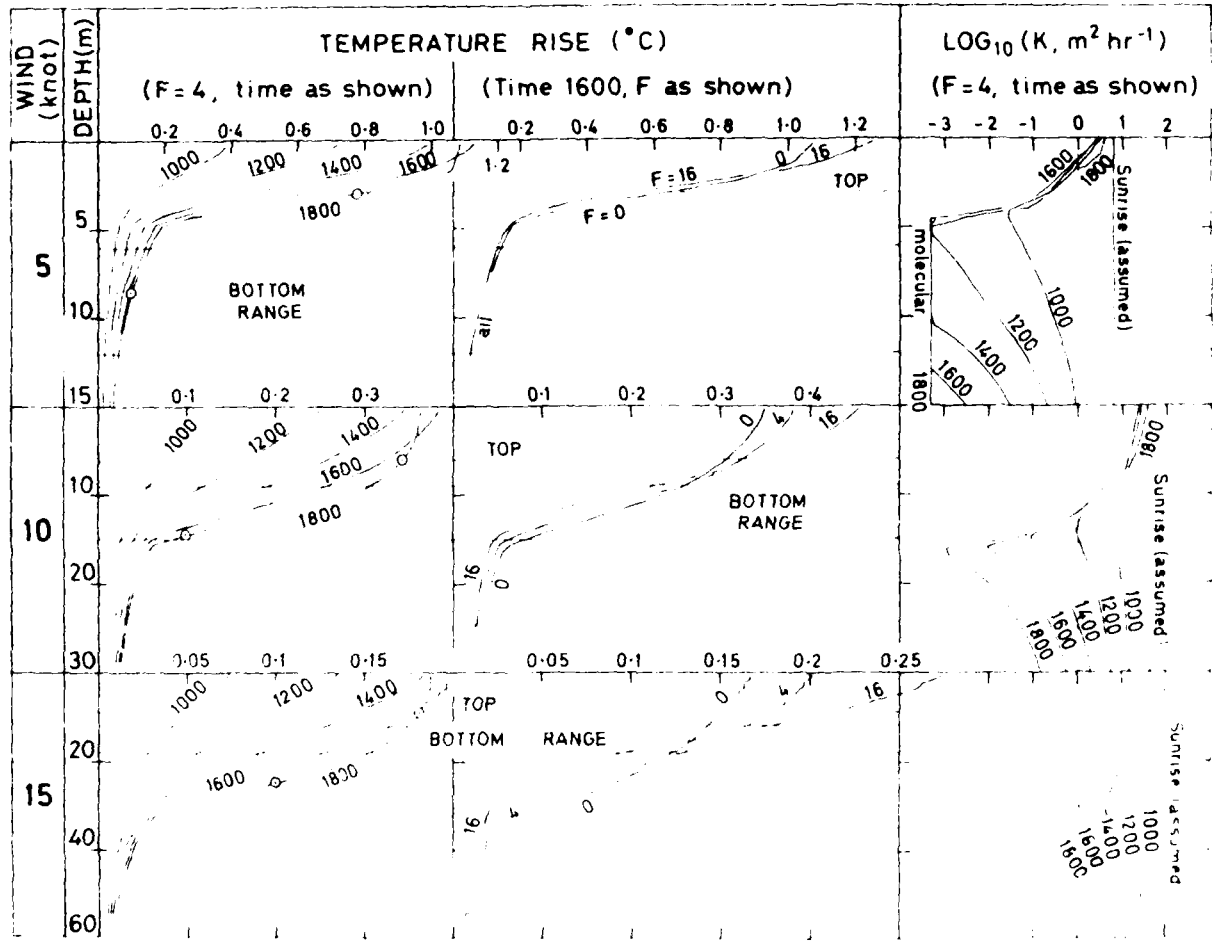

Fig. 9. Modelled results for a midsummer day in latitude 58°N, for wind speeds of 5, 10 and 15 knot. DNOM predictions of depths to top and bottom of transient are superimposed in broken line and shaded band respectively. The right-hand column shows the eddy-diffusivity (K) results.

and depth scales chosen to give all profile sets a broadly similar appearance. The depth to the top of the transient predicted by the DNOM rules is added in broken line. To make a test the intersection of the DNOM line with the 1800 profile is circled; it is seen to be reasonably close to the near-isothermal "front" of the profile for all three wind speeds. This agreement extends to the Tabata et al results also.

The DNOM rules give the transient thickness simply as 3-9 m; the corresponding range of transient bottom depths is added to each diagram as a shaded band. DNOM temperature reporting is to $0.1^{o}C$ so that a rise of this amount may be taken as defining the bottom of the observed transient. Accordingly the intersection of each 1800 profile with the $0.1^{o}C$ line is circled also; it is seen that these intersections lie within the bottom depth ranges for wind speeds of 5 and 10 knot, although not for 15 knot. It is interesting that the only lack of consistency should be at the original 15-knot level, but here we must remember that the whole temperature rise is only twice the DNOM reporting threshold. The third DNOM rule, viz. the unlikelihood of transients at over 15 knot, evidently stems from their smallness rather than their absolute non-occurrence.

Thus the model, originally fitted at wind speeds of 10-15 knot, is seen to respond realistically when the speed is reduced to 5 knot. We can now understand why sonar operational interest is limited to the wind spee range 5-15 knot. At higher speeds the temperature rises are too small to matter; at lower speeds the transient is so shallow as to lie wholly above the sonar projector, thereby providing an overhead "mirror" which if anything helps sound transmission by eliminating surface reflection with its attendant scatter.

The central column of temperature profiles in the figure explores the influence of F. At 10 and 15 knot wind speeds it is much as in Fig. 8,

the speeds being similar. However at 5 knot it falls to a level of unimportance. This means that our F -value originally chosen for high wind speed need not be reconsidered for low speed. Nil-diffusion profiles marked 'N' are added to the diagrams and are seen to coincide with the higher-F profiles beneath the transient.

When the results of Fig. 9, all for $P = 0.5$, are repeated with $P = 0$ it is found that at 5-knot wind speed the iterative solution for F (Section 2d) fails to converge. We have seen that the sensitivity of the modelled temperature profiles to F decreases with decreasing wind speed, implying that the dissipation is decreasing also; this conclusion is later confirmed in Fig. 10. Such could not happen with the $P = 0$ prescription, which ties dissipation to VG^2 independently of wind speed. The implication is that the latter prescription imposes an unrealistic constraint upon dissipation, and should therefore be avoided.

The diffusivity (K) profiles are added to the figure for later comparison with the temperature profiles, but discussion of them is postponed to Section 5.2.

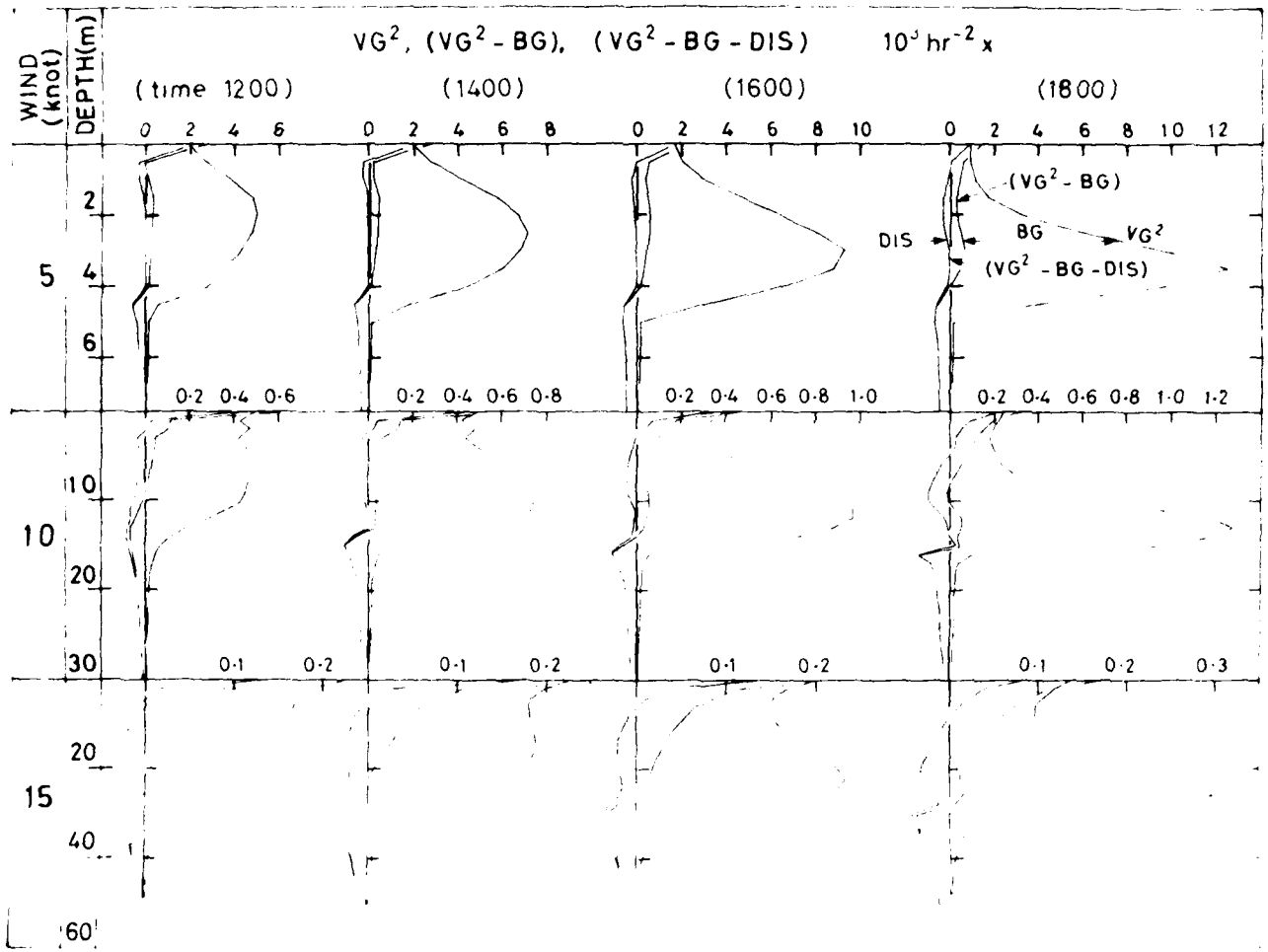

Fig. 10. Variation of VG^2 (square of velocity gradient), BG (buoyancy gradient) and DIS (= ε/K, modified dissipation) with depth. Conditions are as for Fig. 9 with F = 4.

5. Internal behaviour of the model

5.1 The gradient parameters VG^2, BG and DIS

These "bulk system" parameters are of interest for their combined appearance in (9). Since gradients are traditionally noisy and difficult to model, we do this using the idealized data of Section 4 rather than the observed data of Section 3. They are shown in Fig. 10 as functions of depth for the same conditions as Fig. 9, all in the unit s^{-2}. Clarity is improved by plotting the small differences (VG^2 - BG) and (VG^2 - BG - DIS) along with VG^2, with BG and DIS appearing as curve spacings.

The insensitivity of the temperature results to the choice of dissipation prescription has already been mentioned, so the comparatively low levels of DIS seen in the figure come as no surprise. The even smaller significance of dissipation at low wind speed has already been inferred from the central profiles of Fig. 9.

The diagrams show VG^2 and BG increasing with depth to a peak at the bottom of the transient. This peak sharpens as the day progresses. Beneath the transient they collapse abruptly, VG^2 to zero and BG to a low level set by penetrative radiation. We conclude that the downward transmission of momentum and heat due to turbulent diffusion is largely suppressed in this region, for all three wind speeds examined.

5.2 The turbulent diffusivity K

Although K is a central feature of the present work we must not forget that it is an empirical concept unsupported by present-day turbulence theory. The following discussion has been held over pending the assembly of all available evidence.

We refer again to the modelled results of Fig. 9. The range of K-values encountered, five decades in all, makes the use of a logarithmic scale essential. These profiles indicate a major suppression of turbulent diffusivity, developing downwards as the day progresses. At any particular depth within the transient K falls from early morning onwards, reaches a minimum appropriate to that depth, and changes little thereafter. The upshot at 1800 is a steeply-graded K-profile extending from the surface, where there is comparatively little change from the assumed sunrise value, to the transient bottom where K has fallen through several decades. Indeed at 5 knot wind speed the molecular limit is reached over a wide depth range, and at 10 knot it is closely approached. This major reduction of diffusivity at the transient bottom evidently acts like a sheet of highly-insulating material inserted there. The downcoming heat cannot penetrate it and is forced to accumulate above, producing the characteristic half-wineglass-shaped temperature profiles shown at the left of the figure.

It is possible, in principle at least, to infer the K profiles directly from the temperature profiles using (1), i.e. without modelling. Howe and Tait (1969) do this with their observed temperature profile sets, of which a single profile appears in Fig. 1. They are able to follow the fall of K with depth as far as a factor of 15, beyond which the calculation presumably becomes impracticable. The present data is unfortunately not good enough for any such analysis. Nevertheless it seems safe to conclude that wineglass-shaped temperature profiles such as those seen in Figs. 1, 2 and 5 necessarily connote a steep fall in K with depth.

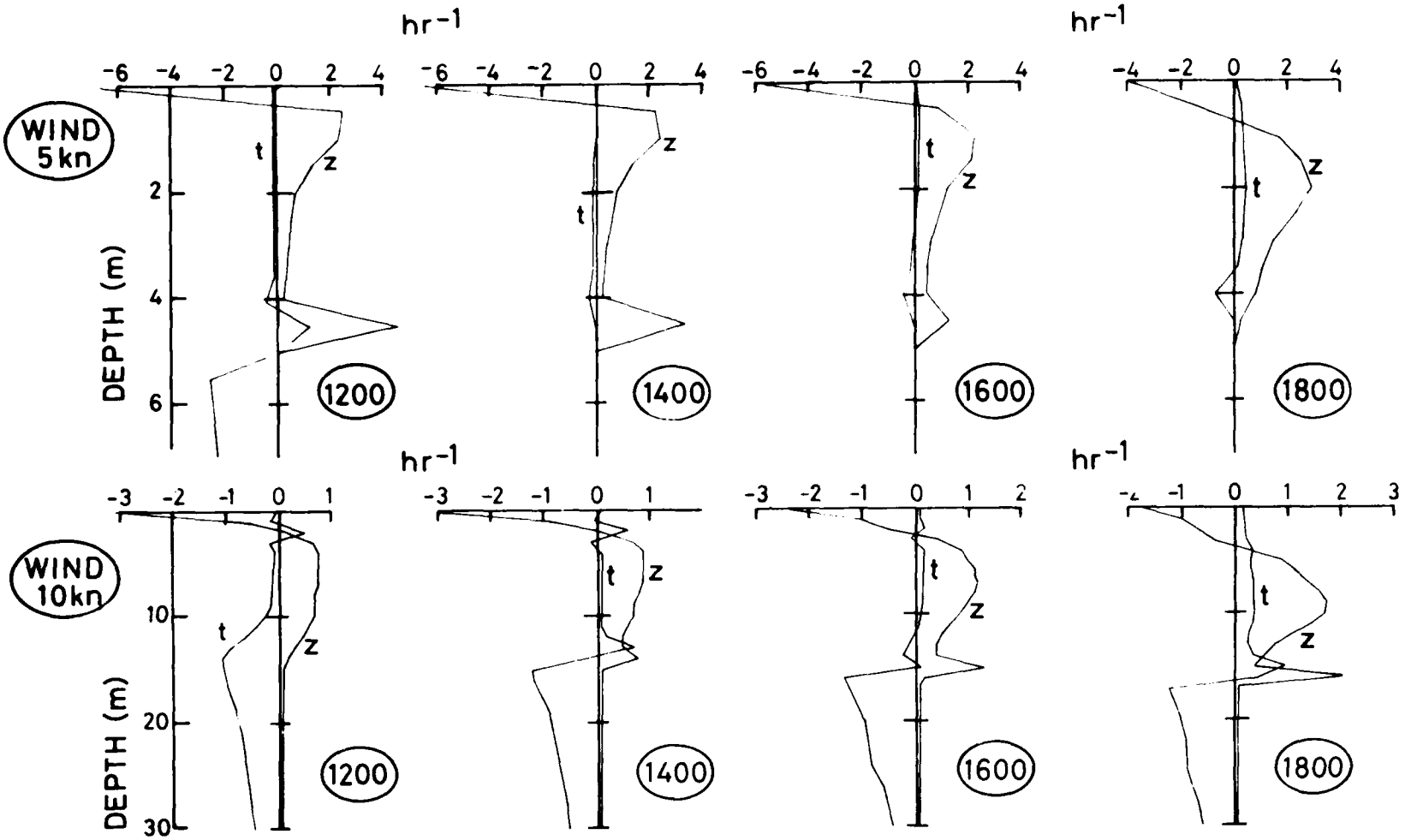

Fig. 11. Variations of $\frac{1}{K}\frac{\partial K}{\partial t}$ and $\frac{1}{K}\frac{\partial K}{\partial z}\left(K\frac{\partial K}{\partial z}\right)$ with depth for two wind speeds, curves marked t and z respectively. Conditions are otherwise as for Figs. 9 and 10.

The K-profiles of Fig. 9 all exhibit minima, becoming sharper as the day progresses, which delineate the transient bottom much better than any feature of the temperature profiles. We see that the transient deepens during the afternoon, and that the major falls in K occur beneath the transient at depths where the latter has not yet arrived. Referring again to (9), change in K is seen to be controlled by the group $(VG^2 - BG - DIS)$. Of these terms only BG persists beneath the transient, as already seen in Fig. 10. It follows that the falls in K are initially caused by radiation alone, penetrating to sub-transient levels.

Within the transient the behaviour of K is entirely different. The virtual coincidence of each set of profiles in this region shows that K remains remarkably constant at any depth, although differing widely between depths. The group $(VG^2 - BG - DIS)$ does not vanish entirely in the region, although small. However (9) shows that it supplies the term $\frac{\partial}{\partial z}(K\frac{\partial K}{\partial z})$ as well as $\frac{\partial K}{\partial t}$; dividing (9) throughout by K makes the relationship clearer. Fig. 11 shows the modified terms $\frac{1}{K}\frac{\partial}{\partial z}(K\frac{\partial K}{\partial z})$ and $\frac{1}{K}\frac{\partial K}{\partial t}$, both in the unit hr^{-1}, for two wind speeds only but otherwise for the conditions of Fig. 10; we see that within the transient virtually all of the drive is taken up by the diffusion term, leaving the storage term negligible. This behaviour is consistent with an ad hoc assumption made for some mixed-layer models, e.g. that of Mellor and Durbin, that net generation may be neglected in the turbulent energy balance. Such an assumption based on actual ocean observations stands by itself, but here we have a model saying the same thing totally unbidden. Some explanation is called for, and one is attempted shortly.

To complete the discussion of K we recall that in the absence of night-time turbulence analysis it is necessary to assume a sunrise value (K_i) uniform with depth, which is estimated here from (10). Fig. 12 shows the effect of varying K_i by factors

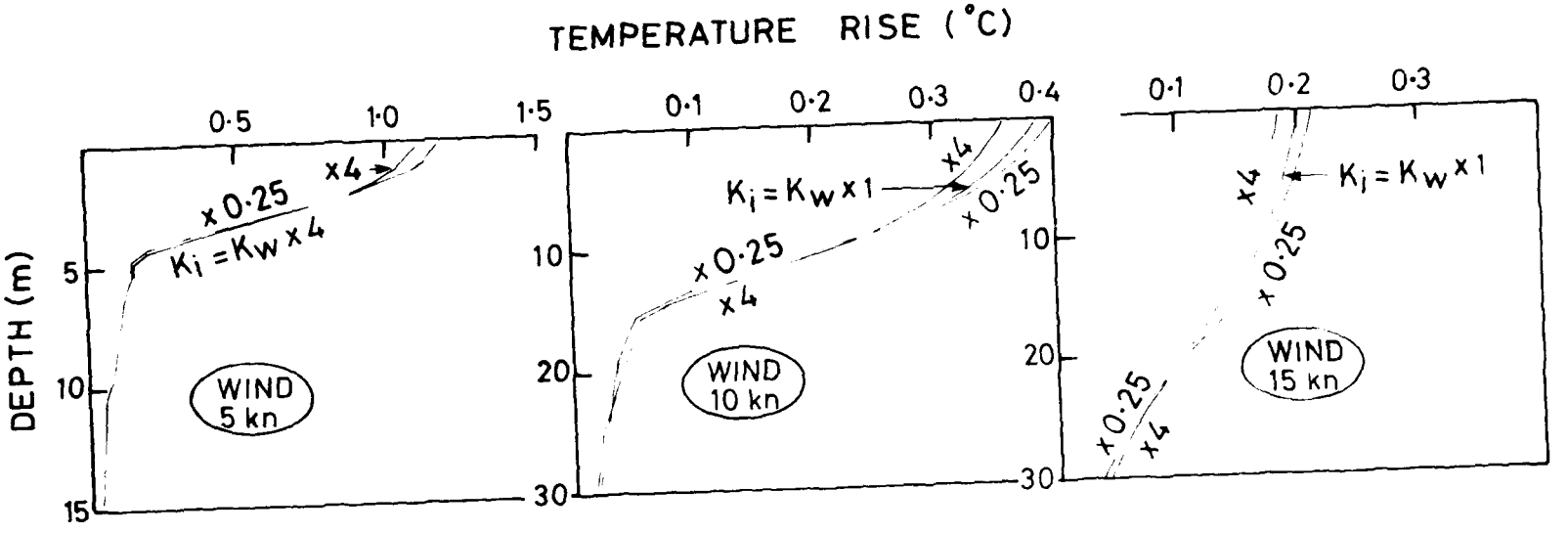

Fig. 12. Temperature profiles for local time 1600 repeated from Fig. 9 with F = 4, showing the effect of varying the assumed sunrise diffusivity K_i by factors of 0.25 and 4.

of 0.25 and 4, on late afternoon temperature profiles. These variations are roughly equivalent to halving and doubling, respectively, the wind speed during the foregoing night. We see that the effect is small at 15-knot wind speed, ranging down to negligible at 5-knot. Thus by late afternoon the transient evolves to a state largely independent of initial conditions. We are fortunate that ignorance of a seemingly key input parameter does not prevent us from modelling transients at all wind speeds of interest.

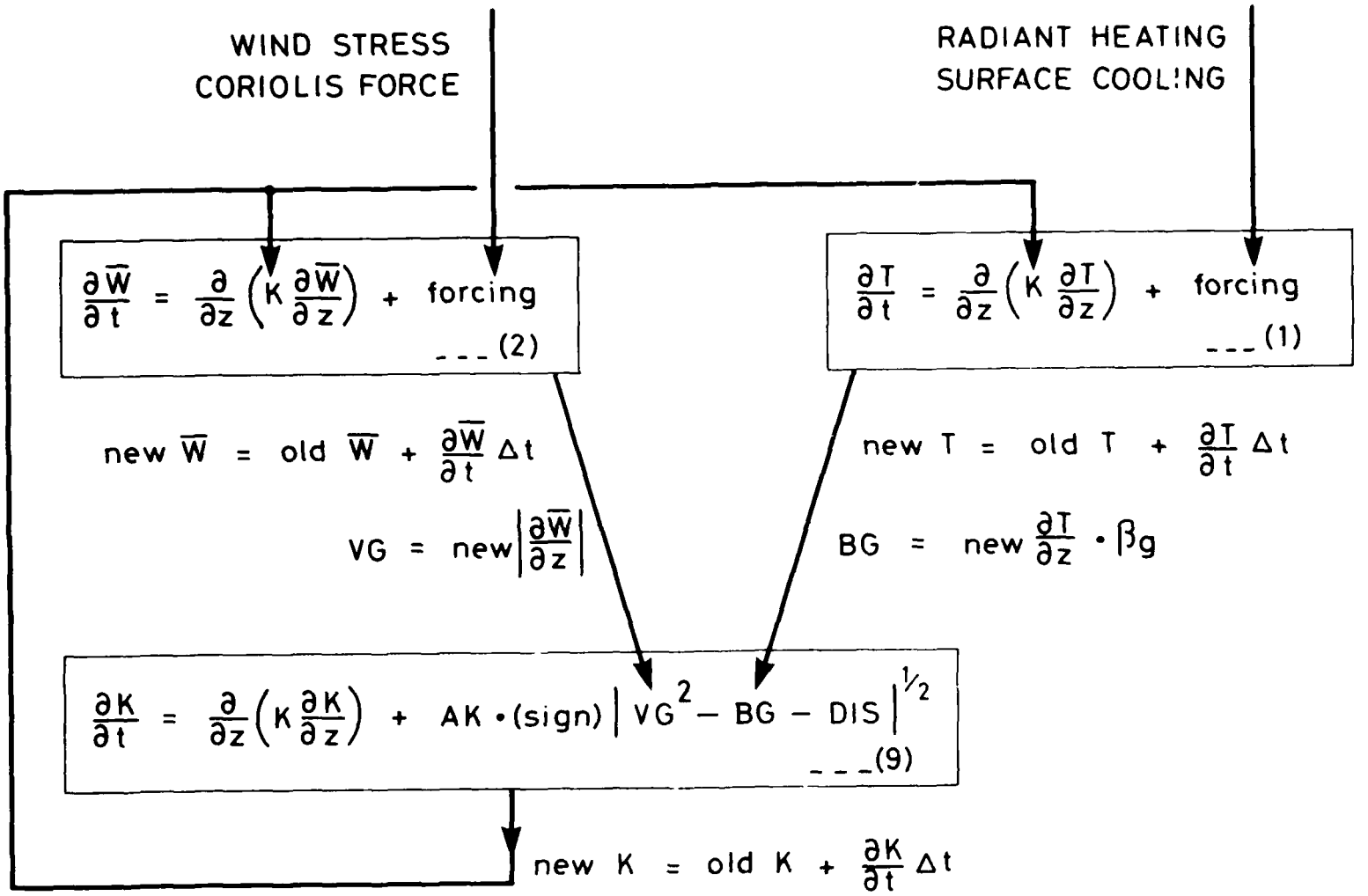

Fig. 14. The diffusion equations for momentum, heat and diffusivity set out in flowsheet form, corresponding to the scheme of numerical solution described in Section 5.

5.3 Feedback loop analogy

We now attempt the promised explanation for the constancy of K at any depth within the transient

The use of only three equations in the model makes its operation easier to understand. Fig. 13 shows the three diffusion equations (1), (2) and (9) assembled flowsheet-wise in a closed loop, corresponding to the actual scheme of computation. We start with (1) and (2) at the top of the figure, externally forced as already described. K plays the same part in both, so that its influence on the outputs VG and BG should be similar. However these enter (9) in opposite senses and in differing degrees; their net effect after processing sets the rate of change of K. We recognise the possibility of a feedback or automatic-control loop here, tending to stabilise K.

To check polarities of changes, consider an increase in wind stress. This increases VG as it enters (9), causing a progressive increase in K. When this is fed back to (2), it tends to "smooth out" the velocity profile and so reduce VG. Hence the polarities are appropriate for stable control. With BG however the reverse applies and the situation is unstable; since BG is always negative the tendency must always be for K to fall. With both tendencies in operation, stability should be possible as long as the influence of VG predominates. Here we recall that VG enters (9) as its square, but BG only linearly. Near the surface where VG and BG are high the possibility of control is most apparent. However at some depth where VG and BG are both sufficiently small, the relative smallness of VG^2 should cause the control loop to collapse.

Since K shows every sign of being controlled at all depths within the transient, we conclude that such a feedback loop is operating; or rather, remembering that we are dealing with a model, that transient

thermoclines behave as though such a loop were operating. This analogue accounts for the near-constancy of K at all depths within the transient. It can also account for the general stability of the results making any form of smoothing unnecessary, and for their insensitivity to the assumed initial value of K. Beneath the transient, however, there is no feedback loop and K can only fall as already noted.

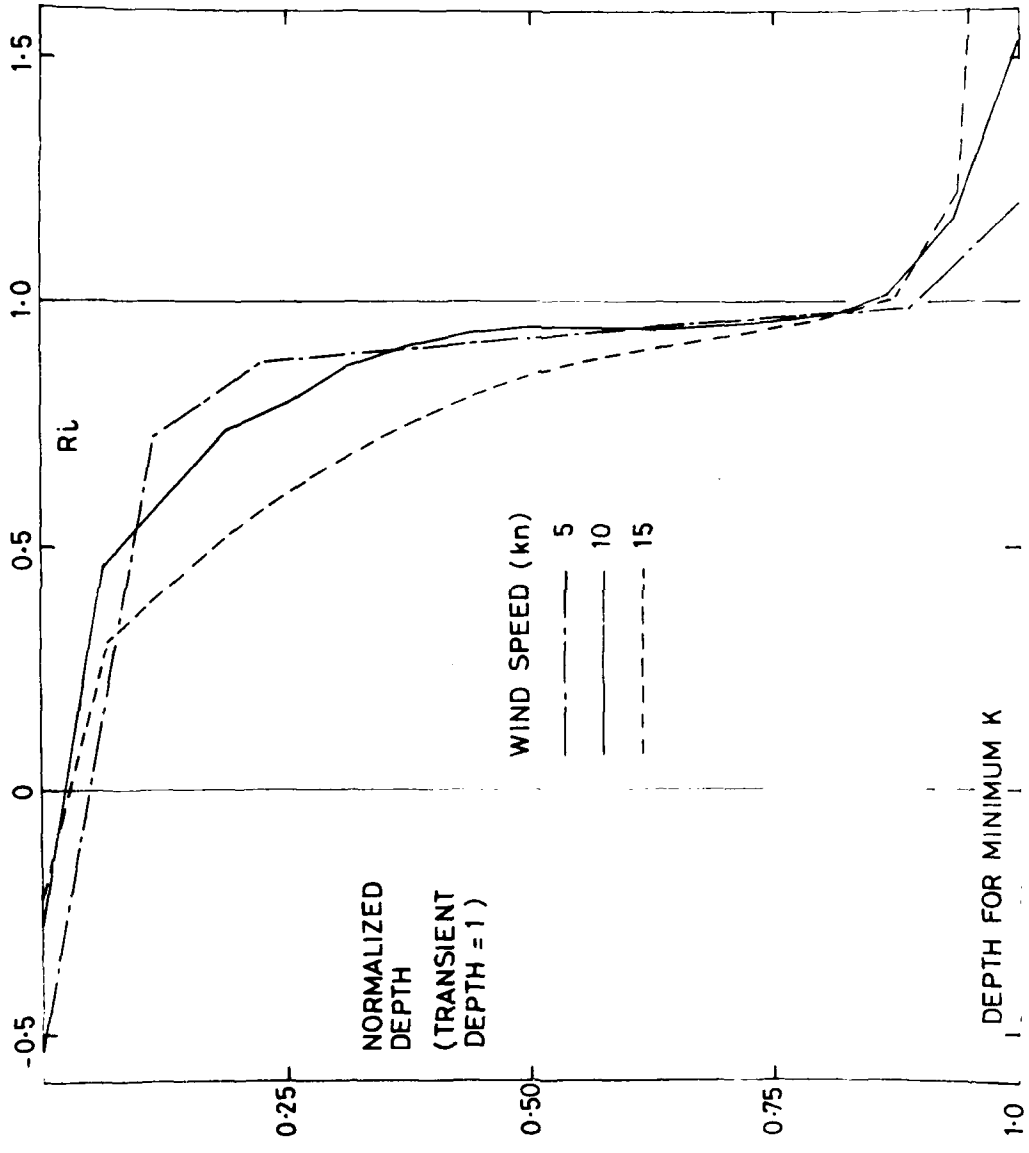

Fig. 14. Ri-profiles for three wind speeds at time 1600. Conditions are as for Fig. 9 with f = 4.

6. Behaviour of Richardson's number

Ri = BG/VG^2 is easily obtained from the results of Fig. 10, and is plotted against depth in Fig. 14 for time 1600 and all other conditions the same. Depth is normalised by expressing it in ratio to transient depth, defined as that for minimum K. Starting from a small negative value due to surface cooling, Ri becomes increasingly positive with depth, steeply with low wind speed and less so with high, approaching 1.0 slowly near the bottom of the transient. Thereafter it increases rapidly, since VG^2 falls to zero but BG does not on account of penetrative radiation.

This regime differs from some others described in the literature. Of these the model of Mellor and Durbin (1975), henceforth MD, is of especial interest because of some close parallels with the present work. It uses the diffusion equations (1) and (2), and ignores turbulent energy storage and diffusion so that (9) reduces to $(VG^2-BG-DIS) = 0$. The dissipation prescription (11) is used, and the approach to calculating the length scale L is that adopted here. K_m and K_h, the differing K's used in the mechanical and heat diffusion equations, are calculated from (12) and multiplied in each case by an algebraic function of Ri. These functions are such that both K_m and K_h fall to quasi-molecular bottom limits if Ri exceeds 0.25 approximately, effectively imposing this upper limit on Ri. Such a limit is also advocated by Turner (1973) from assembled observations of incipient turbulence.

This limitation means, in the present notation, that BG is limited to $0.25\ VG^2$. From the MD approximation $(VG^2-BG-DIS) = 0$ it follows that DIS cannot fall below $0.75\ VG^2$. Hence the turbulence interplay is mainly between generation and dissipation directly to heat, with buoyancy playing only a minor part. We may think of such regimes as mildly stratified, in contrast to the present one of severe stratification where buoyancy plays a major part and dissipation only a minor one.

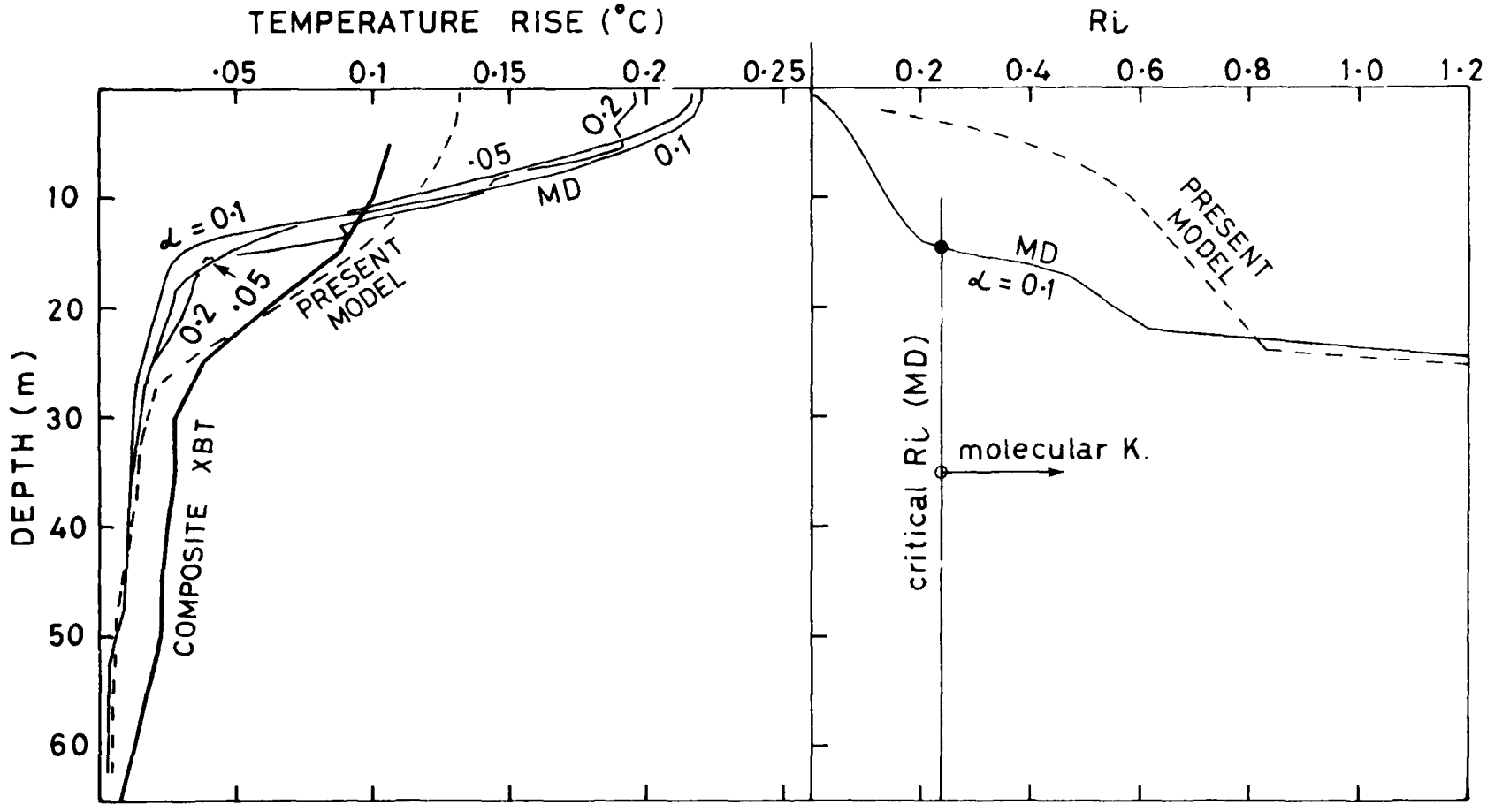

Fig. 15. HMAS DIAMANTINA cruise May 4/5 1976, temperature and Ri profiles at 1600 local time predicted by Mellor and Durbin (1975) model formulation. The central α-value 0.1 is that recommended by MD. The observed and presently-modelled (F = 4) profiles are repeated from Fig. 8 for comparison.

To explore this difference further, the present model is modified by replacing (9) with the MD prescriptions, and then tested against the same data sets as before. The resulting 1600 temperature profile for the HMAS DIAMANTINA 2-day composite data is shown in Fig. 15, with the observed and modelled (F = 4) profiles repeated from Fig. 8 for comparison. It is seen that the MD profile does not fit the observed one so well, being too shallow; halving or doubling the MD constant of adjustment α from its recommended value 0.1 makes little difference. The Ri-profiles are shown at the right, confirming that Ri reaches the values 0.23 and 1.0 near the bottom of the transient as already mentioned. The results for the idealized OWS data are shown in Fig. 16, where the outcome is similar. To put the comparison beyond doubt, we note that the two Ri-curves in Fig. 15 run roughly in the ratio 0.23/1.0 over much of the transient. When the present model is re-run with all buoyancies increased in the ratio $(0.23)^{-1}$, the MD results are found to be closely reproduced.

On the basis of the foregoing evidence, we can only conclude that the natural upper limit of about 0.25, which is sometimes advocated for Ri in the mixed layer, does not apply within transients.

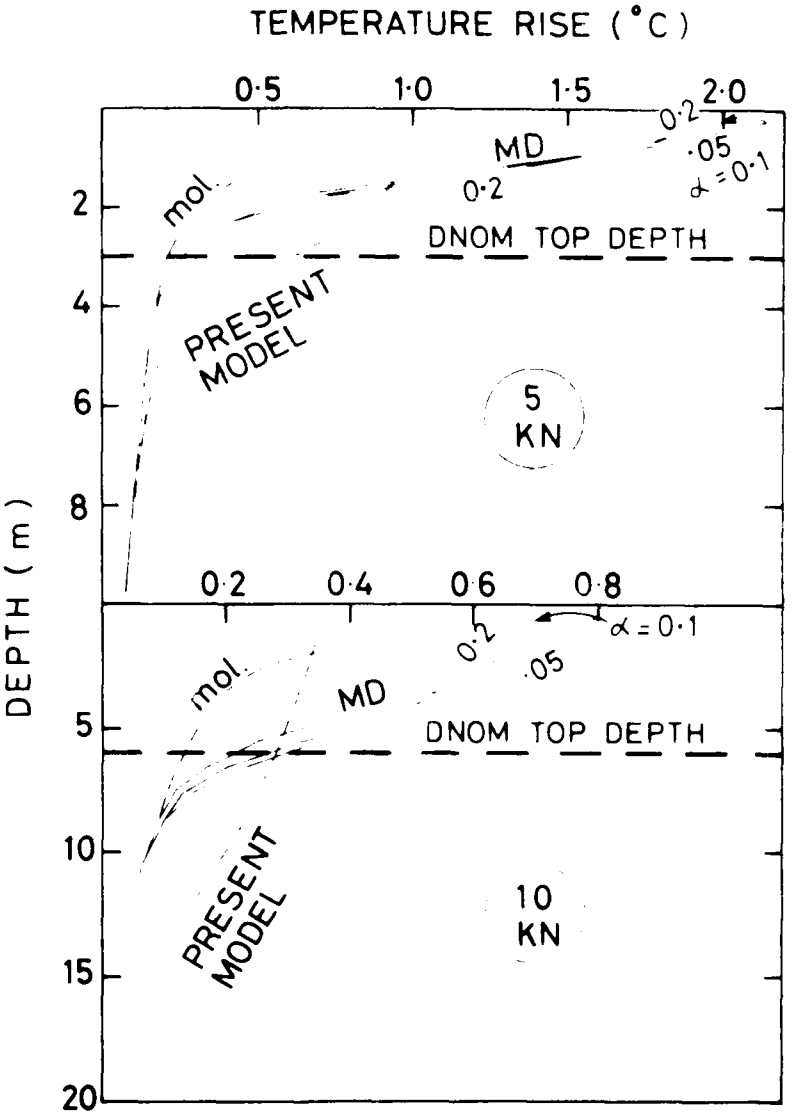

Fig. 16. Temperature profiles for a mid-summer day in latitude 58N at local time 1600, with wind speeds 5 and 10 knot, obtained using Mellor and Durbin (1975) model formulation. The central α-value 0.1 is that recommended by MD. The presently-modelled profile (F = 5) and the DNOM predicted top depth are repeated from Fig. 9 for comparison.

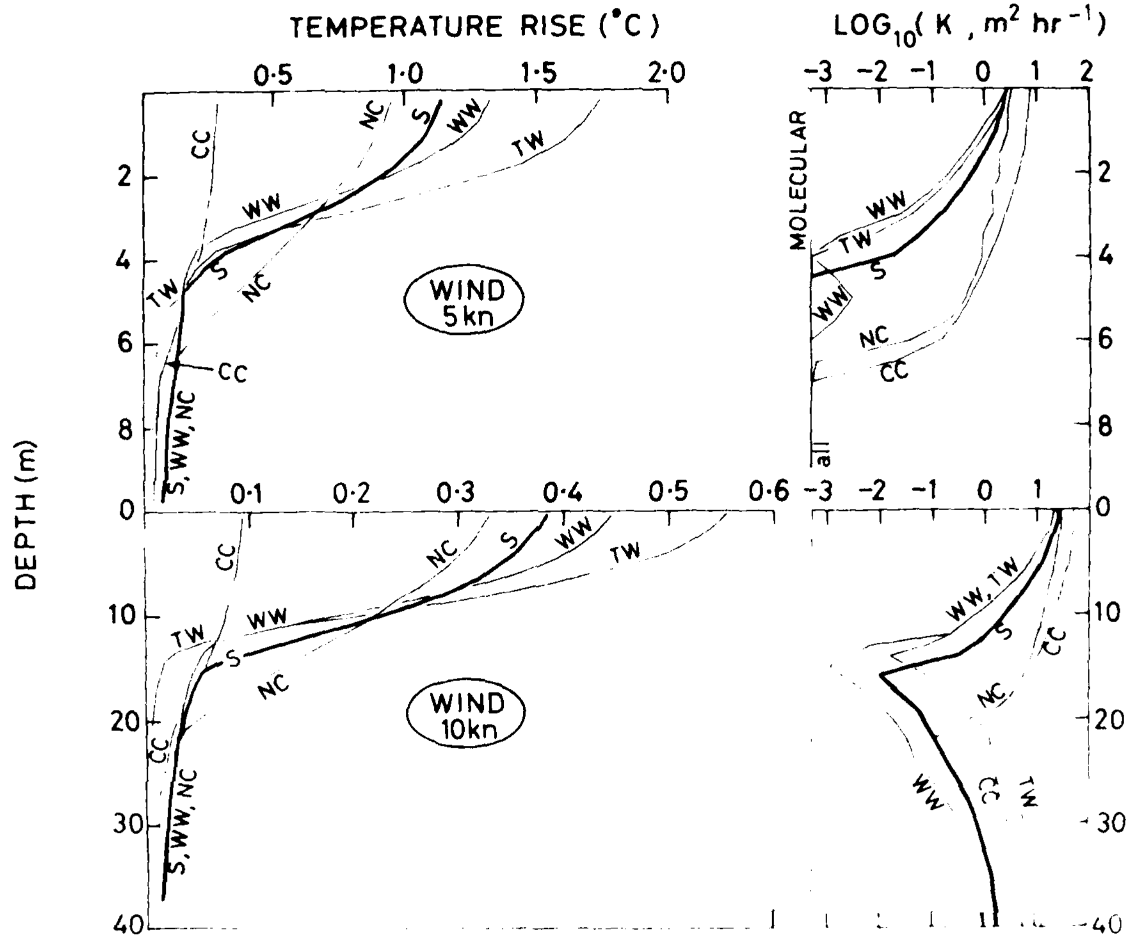

Fig. 17. [illegible] 1600 temperature and diffusivity results [illegible] Fig. 9 (curves [illegible]). The [illegible] curves are for identical conditions except for environmental [illegible] cover; [illegible] water; [illegible] acceleration.

7. Practical predictions of afternoon effect

7.1 Effects of key environmental changes

For the conditions of Fig. 9 (dissipation index P = [illegible] and [illegible]), Fig. 17 shows the 1600 temperature and diffusivity profiles corresponding to the following input variations.

(S) No variation, standard case.

(CC) Cloud cover increased from two-eighths maximum to six-eighths approximately. Radiant heating halved, surface cooling unchanged.

(TW) Turbid coastal or estuarine water, Coastal type 5 instead of Oceanic type Ib (see again Fig. 4).

(WW) Warm tropical water, temperature $30^{o}C$ instead of $15^{o}C$.

(NC) No Coriolis acceleration, location equatorial instead of latitude 53^{o}.

The effect of halving the radiant heat (profiles CC) is naturally to reduce the surface temperature rise, but the reduction is much greater than simple proportionality would predict. This is because the reduction in buoyancy gradient increases turbulence, and so enables the diminished heat supply to penetrate more deeply. At critical depths of 5 m and 17 m for 5- and 10- knot wind speed, the temperature rises are predicted to be slightly increased.

The influence of water turbidity (profiles TW) is clearly a major one. The coastal water category examined here is the central one of five listed by Jerlov (Table XXI); it increases the surface temperature rise by about 50% at either wind speed. The much-increased radiant absorption close to the surface effectively removes the "stem" from the wineglass-shaped temperature profile.

Warmer water (profiles WW) means an increased volume coefficient of thermal expansion, in this instance from .0002 to .0004 C^{-1}, with a proportional increase in buoyancy effects. This naturally makes each temperature profile wider and shallower leaving the radiant stem unchanged.

The removal of Coriolis acceleration (profiles NC) favours the transmission of momentum, so that, conversely, the temperature profiles become narrower and deeper. However the effect is comparatively minor. Again the radiant stem is unaffected; the temperature profiles S, WW and NC are all seen to coincide beneath a critical depth set by the wind speed.

Generally it can be said that the profile of a well-developed transient represents a balance between the two main forcing agents, sun and wind. Any change which alters this balance may be expected to have a major effect on the profile.

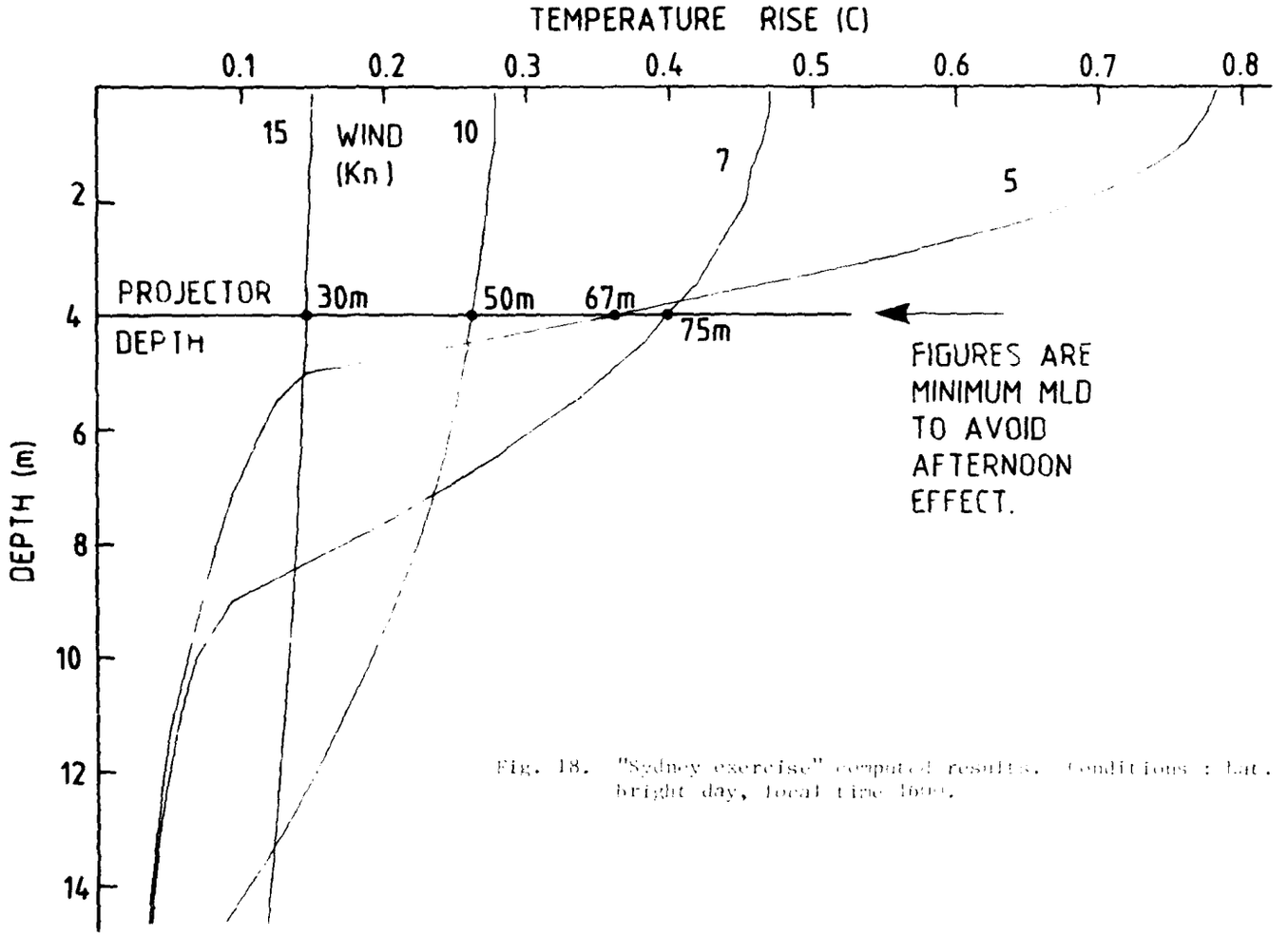

Fig. 18. "Sydney exercise" computed results. Conditions : lat. 34°S, bright day, local time 1600.

7.2 A typical afternoon effect prediction

The following gives some idea of what can be offered at the present stage of development of these studies. In 1981 the RAN Director of Oceanography and Meteorology requested a prediction for late September, to be used in a forthcoming naval exercise near Sydney N.S.W. (latitude 34^{o}S). The basis was to be a fine sunny day, with a full range of windspeeds.

Accordingly the representative windspeeds 5, 7, 10 and 15 knot were selected, and the radiant heating and surface cooling during the day calculated as for Fig. 6. The water optical classification was taken to be Oceanic Ib. The modelled temperature profiles for local time 1600 are shown in Fig. 18. For a bulk mixed-layer temperature of 17^{o}C, the mixed-layer depths giving zero sound-speed excess at a sonar projector depth of 4 m are calculated from Fig. 4 and marked upon the curves; these are the minimum layer depths for which freedom from afternoon effect can be assured.

7.3 Towards a routine prediction facility

At present the prediction procedure consists of three separate parts

(1) A computer program which accepts the hourly forecasts of the meteorological variables, and finds the hourly radiant heating and surface cooling.

(2) The main program which accepts the above, also water optical classification, and finds the hourly mixed-layer temperature profiles.

(3) Fig. 4 or its computational equivalent, converting temperature profiles to sound-speed profiles, over the whole mixed layer. At present only the difference between speeds at projector depth and mixed-layer depth is utilized.

In the short term it is proposed to consolidate (1) - (3) above into a single program. A compiled version will be filed with the CDC 7600 computer, arranged for ready access by the RAN Director of Oceanography and Meteorology.

In the longer term it is clearly desirable for the new facility to be incorporated in the existing range prediction facility AUSRAPS. This question has not yet been addressed.

8. Conclusion

What do we learn from the present studies of afternoon effect?

Firstly we see that it is basically modellable. The types of transient profile actually observed, with their characteristic half-wineglass shapes and strong scaling on wind speed, are realistically rendered. This is achieved using only standard "tools of the trade", viz. the diffusion equations for heat and momentum, and the turbulent energy balance, here all framed in terms of the eddy-diffusivity K. The turbulent energy dissipation prescriptions used are also adapted from the literature.

Secondly, on using dissipation to fit the model to observation we find that only a small amount is needed. Such smallness is shown to connote severe stratification, with gradient Richardson's number close to one, over most of the transient depth. Since this finding contradicts some established mixed-layer thinking, it is as well to review the evidence briefly. Of the HMAS DIAMANTINA data, that for two consecutive sunny days is composited, thus reducing error and uncertainty. The XBT s have no useable temperature base, but when individual profiles of the diurnal set are adjusted for heat input, their "stems" are found to close satisfactorily. The two sets of empirical rules for transient formation are "broadbrush", but are mutually consistent and rest upon large data bases. The finding of small dissipation, made using either data source, is almost a qualitative one and therefore not easily upset. By contrast, it appears that models which limit buoyancy formation to a low level cannot fit the same data so well.

Some interesting aspects of modelled transient behaviour are explored, including a suggestion of feedback loop action tending to stabilize K. Also explored are the effects of varying some key input variables. Generally it may be said that transients represent a balance between the contending influences of wind and sun. Any environmental change which alters this

balance may be expected to have a major effect on transient development.

On the utilization side, some consolidation of computer programs remains to be done, and the question of incorporating the whole facility in AUSRAPS has yet to be addressed.

9. Acknowledgements

Dr W. F. Hunter and Dr I. S. F. Jones of the RAN Research Laboratory read the manuscript and suggested improvements which are gratefully acknowledged. Thanks are due to the HMAS DIAMANTINA cruise leader, Mr K. G. Wood, and his staff, Defence Research Centre Salisbury, and also to the ship's company, for their unstinted co-operation. Further thanks are due to the RAN for making MTV SEAL available to carry out profiling experiments, and to the company of that ship also.

REFERENCES

Bradshaw, P., D. H. Ferriss, and N. P. Atwell, 1967: Calculation of boundary-layer development using the turbulent energy equation. J. Fluid Mech., 28, 593-616.

Bruce, J. G. and E. Firing, 1974: Temperature measurements in the upper 10 m with modified expendable bathythermograph probes. J. Geophys. Res., 79, 4110, 4111.

Director of Naval Oceanography and Meteorology, R. N., 1968: Oceanographic Forecasting in the Royal Navy. MOS(N) Memo 1/68 (1, 2 and 3).

Dillon, T. M., and T. M. Powell, 1979: Observations of a surface mixed layer. Deep-Sea Res., 26A, 915-932.

Friehe, C. A. and K. F. Schmitt, 1976: Parameterization of air-sea interface fluxes of sensible heat and moisture by the bulk aerodynamic formulas. J. Phys. Oceanogr., 6, 801-809.

Frye, H. W. and J. D. Pugh, 1971: A new equation for the speed of sound in seawater. J. Acoust. Soc. Am., 50, 384-386.

Hill, J. W.,1983: A new interpolation method suited to sparse datum points. In preparation.

Hill, J. W., 1980: Progress with modelling diurnal temperature profiles in the upper ocean. 7th Australasian Conference on Hydraulics and Fluid Mechanics, I. E. Aust. Nat. Conf. Pub. 80/4, 381-384.

Howe, M. R. and R. I. Tait, 1969: Some observations of the diurnal heat wave in the ocean. Limnol. and Oceanogr., 14, 16-22.

James, R. W. 1966: Ocean Thermal Structure Forecasting. SP-105 ASWEPS Manual Vol. 5. U.S. Govt. Printing Office, Washington. D.C.

REFERENCES (Con't)

Jerlov, N. G., 1968: Optical Oceanography. Elsevier.

Kaiser, J. A. C., 1978: Vertical and horizontal heat transfer within an oceanic surface mixed layer. Deep-Sea Res., 25, 645-657.

Kundu, P. K., 1980: A numerical investigation of mixed-layer dynamics. J. Phys. Oceanogr., 10, 220-236.

Marchuk, G. I., V. P. Kochergin, V. I. Klimok, and V. A. Sukhorukov, 1977: On the dynamics of the ocean surface mixed-layer. J. Phys. Oceanogr., 7, 865-875.

Mellor, G. L., and P. A. Durbin, 1975: The structure and dynamics of the ocean surface mixed layer. J. Phys. Oceanogr., 5, 718-728.

Munk, W. H., and E. R. Anderson, 1948: Notes on a theory of the thermocline. J. Mar. Res., 7, 276-295.

Nee, V. W. and L. S. G. Kovasznay, 1969: Simple phenomenological theory of turbulent shear flow. Phys. Fluids., 12, 473-484.

Pedersen, M. A., and D. F. Gordon, 1965: Normal-mode theory applied to short-range propagation in an underwater acoustic surface duct. J. Acoust. Soc. Am., 37, 105-118.

Razelos, P., 1973: Methods of obtaining approximate solutions. In: Handbook of Heat Transfer, ed. W. M. Rohsenow and J. P. Hartnett, 4-1 to 4-78. McGraw-Hill, New York.

Romer, J., 1969: Variations de la temperature de la mer au voisinage de la surface. 5th Session of the Commission for Maritime Meteorology, World Meteorological Organisation Technical Note No. 103, WMO No. 247, TP. 135, 97-115.

Shonting, D. H., 1964: Some observations of short-term heat transfer through the surface layers of the ocean. Limnol. and Oceanogr., 9, 576-588.

REFERENCES (Con't)

Stommel, H., K. Saunders, W. Simmons, and J. Cooper, 1969: Observations of the diurnal thermocline. Deep-Sea Res., 16, Suppl., 269-284.

Sverdrup, H. U., M. W. Johnson, and R. H. Fleming, 1942: The Oceans: Their Physics, Chemistry and General Biology. Prentice-Hall New York.

Tabata, S., N. E. J. Boston, and F. M. Boyce, 1965: The relation between wind speed and summer isothermal surface layer of water at Ocean Station P in the Eastern Subarctic Pacific Ocean. J. Geophys. Res., 70, 3867-3878.

Turner, J. S., 1973: Buoyancy Effects in Fluids. Cambridge University Press.

PRIMARY DISTRIBUTION

	COPY NO.
Chief Defence Scientist	1
Deputy Chief Defence Scientist	2
CPAS	3
Superintendent Science and Technology Programmes	4
Director RANRL	5
Librarian RANRL	6-15
Counsellor Defence Science Washington Defence Science Representative London (Document Control Data Sheet Only)	
Naval Scientific Adviser	16
National Library of Australia (via OIC/DEC/DISB)	17
US Defence Technical Information Center for National Technical Information Service (NTIS) (via DISB)	18-29
UK Defence Research Information Centre (DRIC) (via DISB)	30
Director Scientific Information Services (Canada) (via DISB)	31
NZ Ministry of Defence (via OIC/DEC/DISB)	32
Fleet ASW Officer	33
Director of Underwater Weapons	34
Director of Oceanography and Meteorology	35
Staff Officer Oceanography, Hydrographic Office	36
Officer-in-Charge, ASW School HMAS WATSON	37
Librarian HMAS WATSON	38
Senior Meteorological Officer, Naval Air Station Nowra	39
The Joint Directors, Australian Joint Anti-Submarine School Nowra	40,41
Senior Librarian, Defence Research Centre Salisbury	42
Dr. I.S.F. Jones } RANRL	43
Dr. P.J. Mulhearn } RANRL	44
Author	45-50
Librarian Technical Reports Centre Defence Central Library Campbell Park	51
OIC Document Exchange Centre DISB (for microfiche copy)	52
JIO (DDSTI)	53
Librarian H Block, Victoria Barracks, Melbourne	54

Department of Defence

DOCUMENT CONTROL DATA

1.a AR No.	1.b Report Number No.	2. Document Date
AR-002-699	RANRL - TN - 3/82	JUNE 1982 NAV 79

4. Title	5. Security a. document	6. No. of Pages
"AFTERNOON EFFECT" STUDIES, PART I	unclassified	73
	b. title c. abstract	7. No Refs
	unclas. unclas.	25

8. Author(s)	9. Sponsoring Agency
J. WARREN HILL	

10. Corporate Author and Address	11. Authority (as appropriate)
R.A.N. RESEARCH LABORATORY P.O. BOX 706 DARLINGHURST NSW 2010 AUSTRALIA	a. Sponsor b. Security c. Downgrading d. Approval a. N.S.A. b,c. N/A d. D/RANRL J.F. Hunt.

12. Secondary Distribution (of this document)

APPROVED FOR PUBLIC RELEASE

Overseas enquirers outside stated limitations should be referred through ASDIS, Defence Information Services Branch, Department of Defence, Campbell Park, CANBERRA ACT 2601

13. a. This document may be ANNOUNCED in catalogues and awareness services available to

NO LIMITATIONS

13. b. Citation for other purposes (ie casual announcement) may be (select) unrestricted or as for 13.a

14. Descriptors

		15. COSATI Group
meteorology	temperature gradients	
sonar	stratification	
afternoon effect	meteorological data	0810
sound velocity profile		
underwater sound transmission		

16. Abstract "Afternoon effect" is a type of sonar performance loss encountered during the afternoons and evenings of calm sunny days. It is caused by a temperature rise near the top of the otherwise isothermal mixed layer, increasing the sound speed there and so refracting the sound rays downwards, away from the sonar target. The temperature rise profile is governed by wind speed, solar heating and other meteorological factors, so that afternoon effect prediction should become an extension of meteorological forecasting. However there is at present no established method for computing the temperature profile from the meteorological information.

A mixed-layer model is presented which appears to meet this need, subject to further testing. The influences of some key environmental factors are explored. An example of afternoon effect prediction is given, and the next steps towards a routine prediction are indicated.

PF 65

PRECEDING PAGE BLANK-NOT FILMED

This page is to be used to record information which is required by the Establishment for its own use but which will not be added to the NTIS data base unless specifically requested

16. Abstract *(Contd)*		
17 Imprint		
18 Document Series and Number RANRL TECHNICAL NOTE 3/82	19, Cost Code	20. Type of Report and Period Covered TECHNICAL NOTE
21 Computer Programs Used		
22. Establishment File Ref(s)		

END

DATE
FILMED

8-83

DTIC